A Resource for the State of Florida

HURRICANE LOSS REDUCTION

FOR

HOUSING IN FLORIDA:

Roof and Wall Vents Study under Simulated Hurricane Winds

A Research Project Funded by
The State of Florida Division of Emergency Management

Prepared by:

Dr. Arindam Gan Chowdhury, Assistant Professor

Peeyush Kawade & Tuan-Chun Fu, Graduate Research Assistants

Department of Civil and Environmental Engineering

Florida International University

In Partnership with:

The International Hurricane Research Center

Florida International University

September 2009

TABLE OF CONTENTS

1. INTRODUCTION AND BACKGROUND

Natural hazards such as earthquakes, landslides, lightning, floods, windstorms and tsunamis, are great threats to the mankind. Such disasters cost high risk to people and their property. Natural disasters can cost billions of dollars in recovery and repairs. The biggest threats among all such hazards are hurricanes (NSB, 2007; Lott and Ross, 2006). According to the Insurance Information Institute, the 2005 Hurricane Season resulted in $ 57.7 billion dollars in insured losses. A large portion of these losses was attributed to roof damage. Since the mid 1990s the North Atlantic Basin has experienced a substantial increase in tropical cyclone activity fueled primarily by warmer than usual sea surface temperature and decreased wind shear. Goldenberg et al. (2001) concluded that the years 1995-2000 saw the highest mean number of major hurricanes and mean Net Tropical Cyclone (NTC) activity of any 6 consecutive years in the entire 1944-1995 database. The 2004 hurricane season also proved record breaking with four storms affecting the same state, namely Florida, in one season; the last time four storms impacted one state was in 1886 when Texas endured four direct hits. Proportional with increased frequency in hurricane landfall is the increase in damage of economy, destruction of built environment structures (mainly roof structure of residential buildings) and loss of life.

The number of major hurricanes and the annual number of named storms has been shown in Figure 1. It appears that in last 3 decades there is an increasing trend in the occurrence of storms, which together with a growing coastal population presents a new challenge for the Civil and Wind engineering communities. According to the Annual Summary for the Atlantic Hurricane Season 2004 (National Hurricane Centre), losses due to hurricanes in the 2004 season were estimated to be $ 45 billion and they also

accounted for 3100 casualties, 60 of which happened in the United States (Frankling et al., 2005). The growth of hurricane-induced losses from $1.3/year pre-1990 to $36B/year post-2000 is a direct result of over 50 years of accumulated socio-economic decisions to invest in physical infrastructure and community development along coastlines, where now 50% of the US population lives within 50 miles of the seaboard (National Academy of Sciences, 1999). The 2005 Hurricane season also produced strong storms with devastating power, such as Wilma and Katrina, causing losses over $ 100 billion. The magnitude of the storms can't be changed, but the magnitude of the impact on population and damages caused by them might be minimized by improving construction techniques and materials and by increasing the general awareness of the risks imposed by this natural phenomenon.

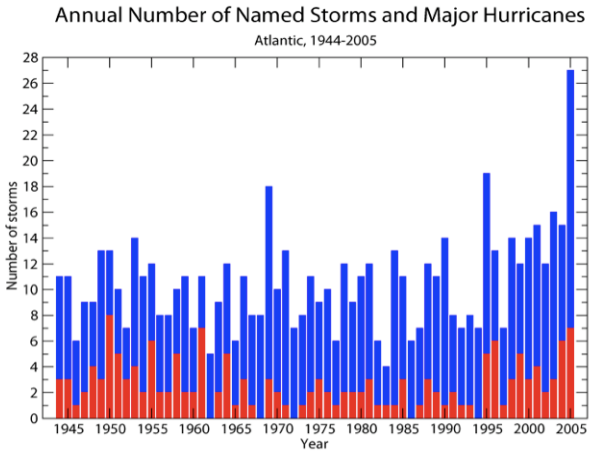

Figure 1. Annual number of named storms (BLUE) and major hurricanes (RED) 1944-2005 (source: National Climatic Centre, 2006)

Roof and Wall Ventilation:

Typical household activities can cause serious problems to a roof and attic if proper roof ventilation is not provided. For example, in summer, heat build-up encourages the premature aging and cracking of wood and other roofing materials. Unwanted heat also can transfer back down into living areas – which reduces energy efficiency. Similarly, in cold weather, warm air generated by laundry, showers, dish washing and cooking can linger in the house and cause moisture build-up. The only way to combat these problems is to have a balanced ventilated wall and roofing system. That means it's important to have proper ventilation, plus the appropriate amount of attic insulation to maximize performance.

In a balanced system, wind blowing over the ridge creates negative pressure that draws the warmer air out of the attic. Replacement air then enters through underside of the eave or soffit vents, bathes the underside of the roof, and exits through ridge, roof or gable vents. Even without wind, the natural convection action of rising warm air maintains a continuous airflow along the underside of the roof.

Proper ventilation—along with attic insulation—helps maintain a comfortable temperature inside a home, increase energy efficiency, prevent moisture damage and contribute to the longevity of a roof. However the vents are subjected to wind loading and can be the path for water infiltration during hurricane events. Very limited research has been performed on water intrusion through various types of vents under differential pressures. The current project focuses on the performance of vents under simulated hurricane effects.

2. TEST METHODOLOGY:

Florida Building Code (FBC, 2007 – Section 1523) defines the minimum testing requirements for substrates, roofing components, roofing systems and roofing assemblies. The current study is based on full-scale holistic testing of roof vents which provides advantages over component testing as the whole building structure incorporated with vents is subjected to wind and wind-driven rain field engulfing the structure and thus producing realistic aero-hydrodynamic effects. A full-scale model representing a typical low-rise building was constructed for the testing purpose. Roof and wall vents were installed on the building model. Wall of Wind (WoW) (6-fan system) was used to determine wind forces and water intrusion through the vents. Pressure differentials for the vents were obtained from a simultaneous project (Bitsuamlak and Tecle, 2009). Transducers installed on the vents measured the wind-induced loading and data was acquired using the lab view data acquisition software.

Tests were performed with and without wind-driven rain. Any failure mode and/or water intrusion was recorded. Failure modes of and water intrusion through different kinds of vents were studied and correlated to the wind speed and wind-driven rain intensity. This research provides information that will help to address significant vent damage and secondary water infiltration and debris generation occurring related to the poor performance of roof and wall vents.

3. THE WALL OF WIND (WoW) TESTING APPARATUS:

3.1 Full scale testing equipment -- Wall of Wind (WoW)

Built by the International Hurricane Research Center (IHRC), the Wall of Wind (WoW) hurricane simulator is a full-scale destructive testing apparatus located at FIU's Engineering Center Campus. This machine is capable of testing a full-scale low-rise building model. The WoW comprises of a 6-fan array and was used for this study. In its original configuration, the 6-fan WoW had the capability of generating 125 mph wind speeds at the exit of the contraction, corresponding to a middle range Category 3 hurricane as defined by the Saffir-Simpson hurricane intensity scale (Huang et al., 2009). This integrated system couples hurricane like winds with wind-driven rain in a controlled environment to allow realistic simulation of hurricane wind and rain interactions with buildings (Bitsuamlak et al., 2009).

The design for the 6-fan WoW consisted of six individual fan modules. Figure 2a & 2b shows the 6-fan WoW front view and side view. The cross-sectional area of one fan module measured 2.44 m (8 ft) high x 2.44 m (8 ft) wide, and these six modules were stacked into a 2x3 array, giving the 6-fan WoW a total flow field measuring 4.8 m (16 ft) high by 6.7 m (22 ft) wide. The engine frames were designed and built to contain carbureted Chevrolet 502 big block crate engines (Figure 3). Century Drive System SH3 2:1 counter rotating drive units were mounted to each engine, with a set of 4- bladed Sensenich composite airboat propellers installed on the front propeller hub (closest to the engine) and a set of 3-bladed Sensenich composite airboat propellers installed on the rear propeller hub (farthest from the engine). The counter rotating setup was made because it

reduces the amount of propeller-generated swirl in the flow, and it reduces the overall propeller torque on the engine. Figure 4 a, b & c shows the setup of fans and blades and different components of WoW relevant to the present testing.

(a)

(b)

Figure 2. Six-Fan Wall-of-Wind (a) Front View (b) Side View

Figure 3. Chevrolet 502 big block crate engines

(a)

(b)

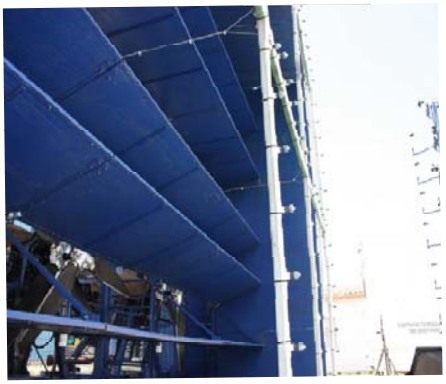

(c)

Figure 4. (a) Setup of fans and blades,
(b) Control System for the fans and
(c) Planks Setup

3.2 WoW flow management techniques

Passive Controls:

Passive controls include (1) a contraction all around the 6-fan system used to point the generated wind towards the test model (Figure 2 a, b); (2) an outer frame installed outside the 6-fan WoW model acting more like a bell-mouth; (3) raising the full-scale six fans by 0.41 m (16 in) above the ground to create a wind speed gradient at the bottom, thus simulating an Atmospheric Boundary Layer (ABL) like flow; and (4) installing five horizontal planks with different inclinations to increase the wind speed with increasing height and generate an ABL-like flow. The three bottom horizontal planks were used to redirect the flow from the bottom fans to the top fans. To optimize the locations and inclinations of the planks, series of experiments were carried out. The optimal configuration was determined with the planks located at the heights of 40 in, 70 in, and 94 in (1.016 m, 1.768 m and 2.376 m) with the inclinations of -0.5^0 (pointing down), 17^0 (pointing up), and 17^0 (pointing up), respectively. Two additional planks were installed in the upper area to improve the flow. A series of combinations of plank locations and angles were tried to produce the targeted ABL-flow. The configuration with five planks (i.e.; -0.5^0, 17^0, 17^0, 0^0 and 0^0 inclination with centers at z= 40, 70, 94, 137, 168 in, respectively) generated the target ABL profile and hence was adopted (Huang et al., 2009).

Active Controls:

To further enhance the turbulence generation and gust effects for the WoW, rapid variation of the fan engine speed was achieved by servo-control through multiple sinusoidal control functions by adding low frequency fluctuations. Combinations of low-frequency quasi-periodic waveform signals were designed based on real tropical storm data taken from the Florida Costal Monitoring Program (FCMP), and were used to control the rotational speed of the fans. These active controls helped to improve the turbulence intensities as well as the power spectral densities and the gust factors. Wind flow characteristics generated by a combination of the passive and active controls that are used in the present study are shown in Figure 5 (Huang et al., 2009).

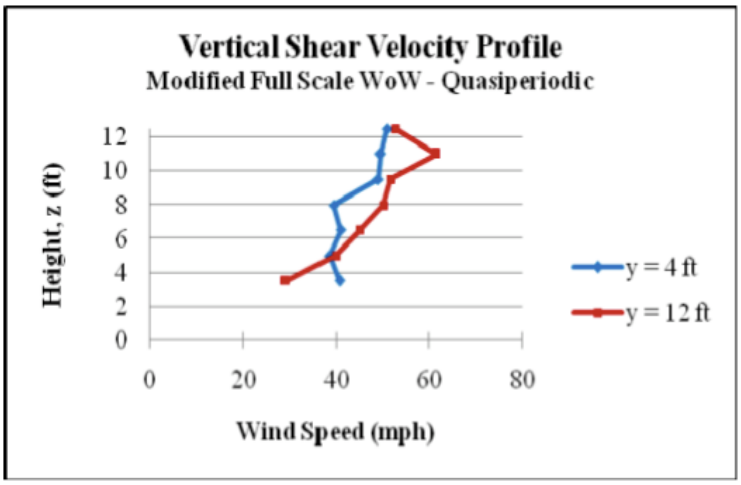

(a)

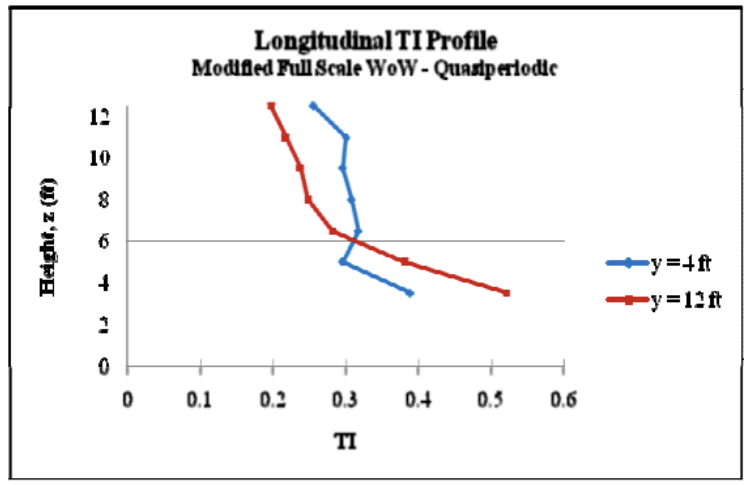

(b)

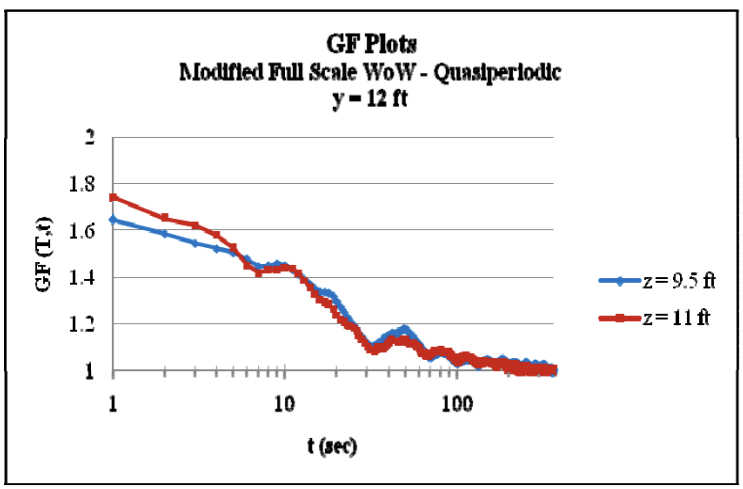

(c)

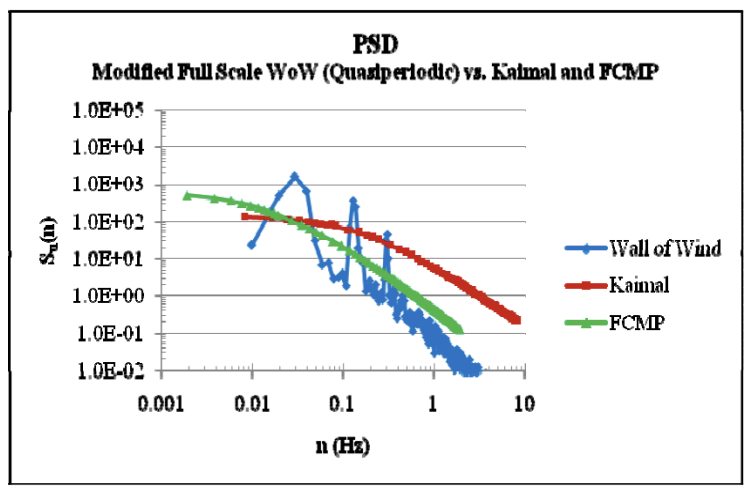

(d)

Figure 5. (a) WoW Vertical shear velocity profile
(b) WoW Turbulence intensity profiles for the longitudinal direction of wind
(c) Gust factors at height = 9.5 ft and z = 11 ft
(d) WoW power spectral density Vs. the Kaimal and FCMP Curves

3.3 Water Injection System

A steel frame was fabricated and installed in front of the 6-fan units. A grid of four columns and three rows of Tee Jet spray nozzles, joined together with high pressure hosing, were mounted vertically to this frame. Figure 6 a, b & c shows the steel frame system and its details. The spray nozzles on each line were spaced 18 inches apart. In this system, two different types of spray nozzles are used: (i) on inner lines, 8005VX nozzles release 0.5 gallons of water per minute (0.5 gal/min) at 40 psi, (ii) on outer lines, 8003VX nozzles that release 0.3 gallons of water per minute (0.3 gal/min) at 40 psi. A gasoline powered pump (Figure 7) effectively works to overcome the head and preserve the water pressure in the spray injection nozzles located on the upper rows. Water meters are used (Figure 8) to calibrate water rate to generate a specific water rate. Water for the injection system is stored in a 550 gallon agricultural grade horizontal leg tank (Figure 9). The pressurized pump feeds the grid and spray nozzles, spraying the water at specified rate, while the fans blow the wind simultaneously (Bitsuamlak et al., 2009).

(a)

(b)

(c)

Figure 6. (a) WoW, Steel framing and setup
(b) Spray nozzles used for water injection system
(c) Water spray from the nozzles

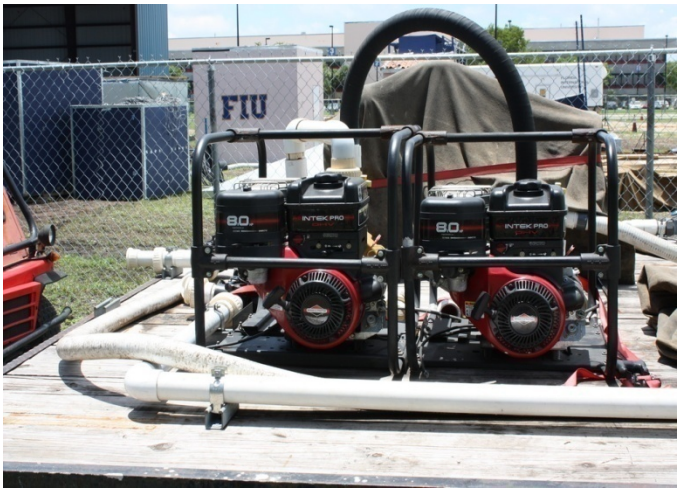

Figure 7. Gasoline powered pump

Figure 8. Water meter

Figure 9. 550 gallon agricultural grade horizontal leg tank

4. EXPERIMENTAL APPROACH:

4.1 Roof and Wall Vents Setup and Instrumentation

The experimental setup considered two common roof types mounted atop a 9 ft x 7 ft x 7 ft (length x width x height) building model. Prior to mounting the roof specimens onto the building model, each roof was prepared with 30 lb felt paper underlayment

(Figure 10 a & b), covered with 5-tab architectural shingles, and outfitted with the roof and wall vents of interest. For the scope of this study, a 10 x 4 x 8 inch (length x width x height) gooseneck vent, a 12-inch turbine vent, a shingle vent II ridge vent, and 16 x 6 inch soffit vents were installed on both the gable and hip roof specimens. Additionally, the gable roof specimen contained a 12 x 12 inch rectangular gable end vent. Figure 11 shows the installation of the roof vents on the gable roof and hip roof specimens. Each of the vents had Notice of Acceptance or Product Approval.

(a) (b)

Figure10. (a) Gable roof prepared with 30 lb felt paper underlayment
(b) Hip roof prepared with 30 lb felt paper underlayment

Figure 11. Turbine vent, goose neck vent, and ridge vent installed on the gable & hip roof specimens

4.1.1 Pressure Testing:

A 16-channel Scanivalve Digital Sensor Array DSA 3217/16PX measured the pressure time histories along the turbine and gooseneck vents according to the tap layout. The Scanivalve device was installed within the attic space of the roof specimens. The pressure taps on the turbine and gooseneck vents were created by gluing small square tabs made of wood or hard plastic onto the inside of the vents at every pressure tap location. Next, a 5/64 inch diameter hole was drilled out at each tap location, and a piece of 5/64 inch outside diameter (O.D.) tubing was glued into each tap. The tubing length between the pressure taps and the Scanivalve was no longer than three feet to minimize signal distortion developed by the tubing. Pressure taps were also installed to measure the external and internal pressure differential across the ridge vent, gable end vent, and soffit vents (Bitsuamlak and Tecle, 2009). Wind attack angle and the locations of the pressure taps on turbine and goose neck vent are shown in Figures 12 and 13. Figure 14 a to g, shows other details related to the different vents and pressure measurement

instrumentation. For the pressure taps installed near the soffit and gable end vents, 5/16 inch O.D. copper taps were installed. Setra 265 differential pressure transducers measured the pressure time histories at these locations. Reference pressure tubing for these transducers was installed in the manner described at length in Blessing (2007). The Setra 265 pressure transducers were connected to an NI 9074 cRIO module, with NI 9205 32-channel analog voltage inputs. Figure 15 shows the NI 9074 cRIO (Compact RIO). NI Lab View software was used to collect and record the data. All measurements were sampled at a rate of 100 Hz during the experiments.

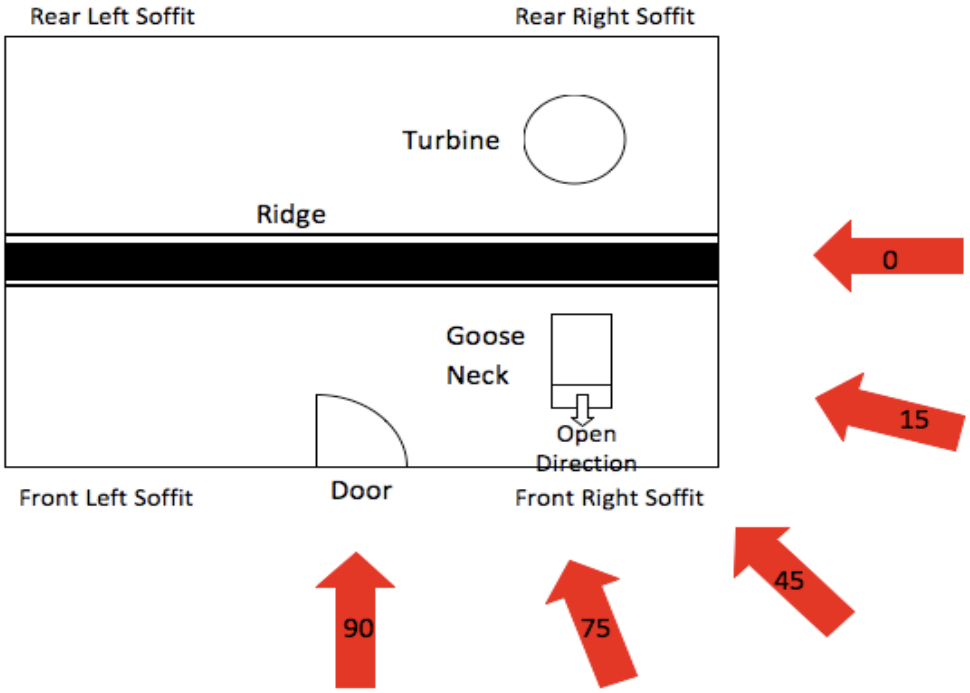

Figure 12. Wind angle of attack and turbine/goose neck vents locations

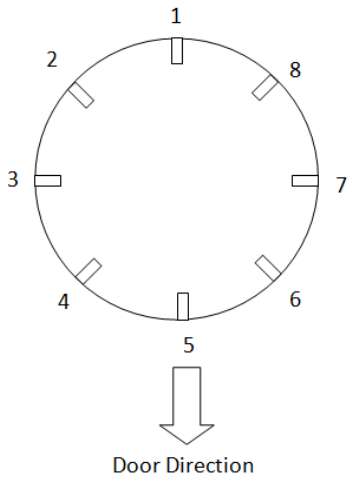

(a)

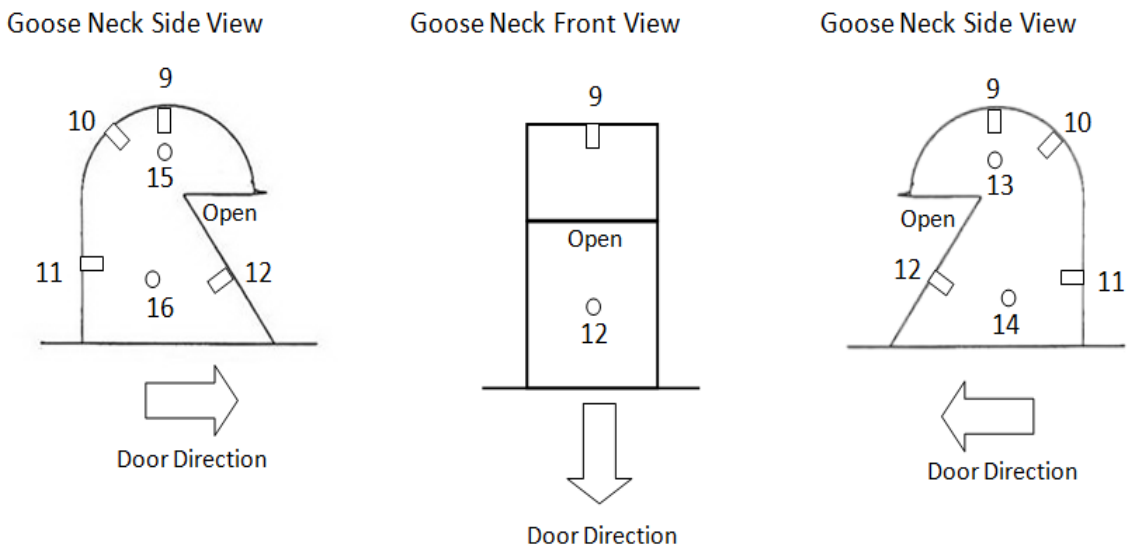

(b)

Figure 13. Pressure Tap Locations: (a) Turbine (showing cross-sectional locations of the pressure taps), (b) Goose Neck Vent

a)

Figure 14. (a) Pressure tubing installed within the turbine vent base
(b) Pressure tap installed on gable vent
(c) Turbine vent setup on the roof specimen
(d) Goose neck vent setup on the roof specimen
(e) Pressure tab installation on soffit vent
(f) Transducer installation on soffit vent
(g) Soffit vent installed on a gable roof specimen

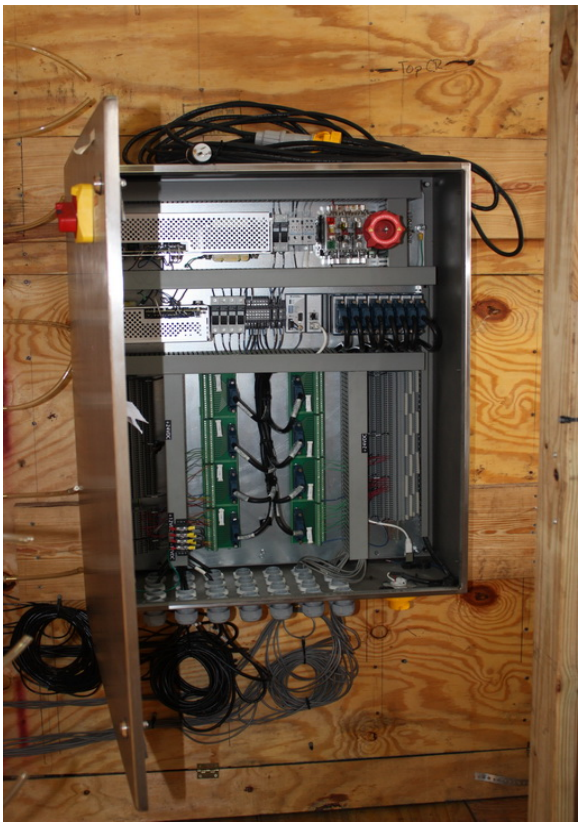

Figure 15. NI 9074 cRIO (Compact RIO)

4.1.2 Water Intrusion Testing:

Water intrusion tests were performed on the gable roof to quantify the volume of water entering the attic space through each of the vents installed on the roof. A piece of plastic sheeting was attached to the perimeter of the goose neck, turbine, ridge, and gable end vents to contain the water entering the attic space through each vent, and direct the water toward collection buckets for each vent. The plastic sheeting was secured with the vents with aluminum tape, as shown in Figure 16 a to d. For the turbine and gooseneck vents, aluminum pans were placed underneath the plastic sheeting arrangement to collect the incoming water. For the ridge vent, a 4-inch I.D. PVC pipe was cut in half to create a trough that would collect the water after intrusion, and direct it into eight measuring

buckets. Plastic sheeting was installed between the ridge vent and the PVC trough to ensure no water would bypass the collection system. A similar arrangement was constructed for the soffit vents (Figure 16 e). Air was allowed to exit the collection pans and the collection buckets for each vent, so that the airflow passing through the vents was not hindered by the collection system. Figure 17 shows all the containers used for the experiment.

Figure 16 a. Water collection setup for the gooseneck vent

Figure 16 b. Water collection setup for turbine vent

Figure 16 c & d. Bucket setup for ridge vent and setup for gable end vent

Figure 16 e. Setup for soffit vent.

Figure 17. Aluminum pan used for water collection.

4.2 Experimental Procedure

4.2.1 Pressure Testing:

During this study, the roof vents were tested at five different angles with respect to the WoW flow field (Figure 12): 0, 15, 45, 75, 90 degrees. A 3-minute, quasiperiodic waveform was used to generate the wind conditions for each test (refer to Liu, 2008).

Prior to running the experiment at each angle, a 3-min baseline of pressure data was taken. During the quasiperiodic profile, 3 min of data was collected. Following each experiment, a second 3-min baseline was performed. All data were sampled at 100 Hz. Both baseline datasets were used to establish the environmental conditions, and were averaged together and deducted from the actual data collected during the WoW run to determine the wind-induced pressure. Figures 18 and 19 show the specimen setup for experimenting.

Figure 18. Experimental setup with turbine, goose neck and gable end vents.

Figure 19. Experimental setup showing gable end and soffit vents.

4.2.2 Water Intrusion Testing:

For the water intrusion testing, a flow rate of 19 in/hr (maximum flow rate at WoW) was used across the WoW flow field. The same three-minute quasiperiodic engine waveform was used for these experiments. Once the profile was initiated, an operator engaged the WoW water-injection system for the duration of three minutes. After the profile was completed, the water collecting containers were removed from the building and weighed on a digital scale. The weight of each dry container was subtracted from the weight of the container with water to determine the amount of water intrusion for each vent. Figure 20 shows the water intrusion test.

Figure 20. Water intrusion test on gable roof

5. RESULTS AND DISCUSSION

5.1 Pressure Test Results:

Figure 21 shows the time history data of typical pressure test. Each test duration is 3 minutes for both baseline and profile parts. Coefficients (C_p) of mean and peak pressures are calculated based on the time history data. The mean wind speed at the mid height of the roof is used for pressure coefficients calculations.

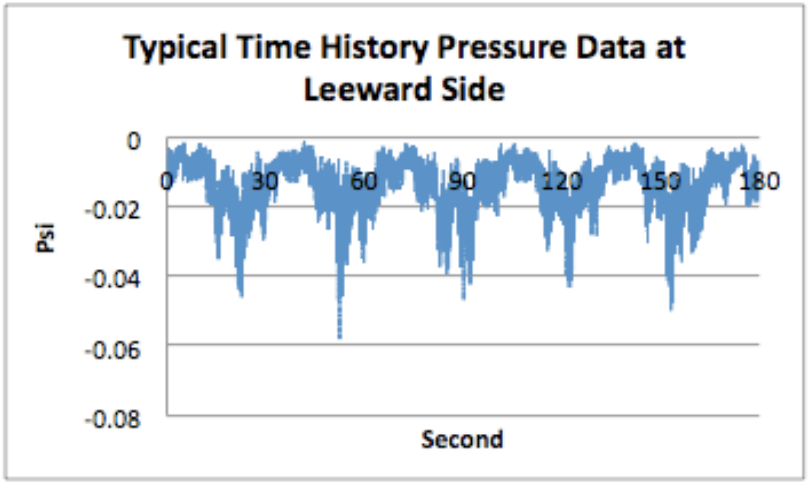

(a)

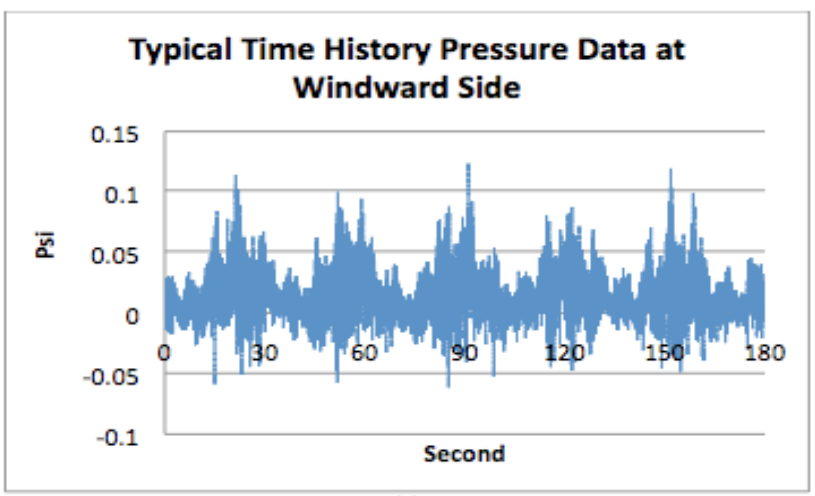

(b)

Figure 21. Typical time history pressure data at:

(a) Windward side and (b) Leeward side

5.1.1 Gable Roof Results:

The following figures show average, standard deviation, maximum and minimum pressure coefficients for external pressure taps on the turbine and goose neck vents. The maximum C_p values are obtained at the pressure taps facing the wind attack direction. For example, for 0 degree wind attack angle, turbine tap #7 and goose neck tap #13 are the taps facing to WoW. Therefore, the maximum C_p values were observed for #7 and # 13 windward taps.

1) For "0" degree angle of attack:

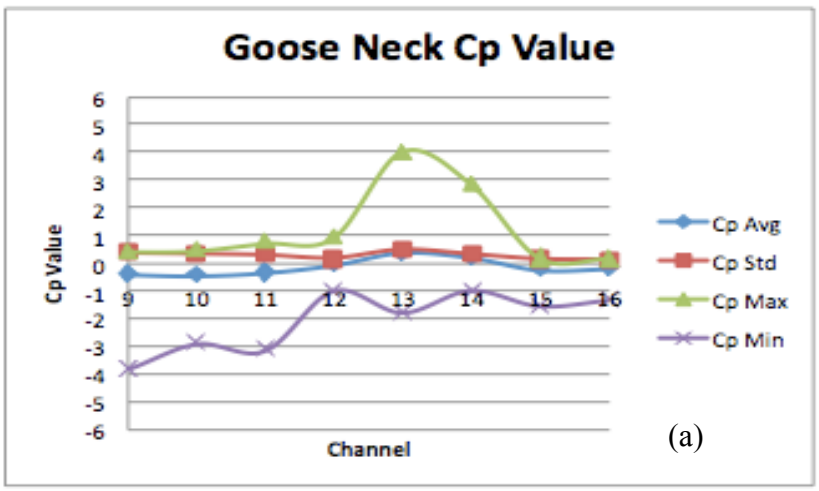

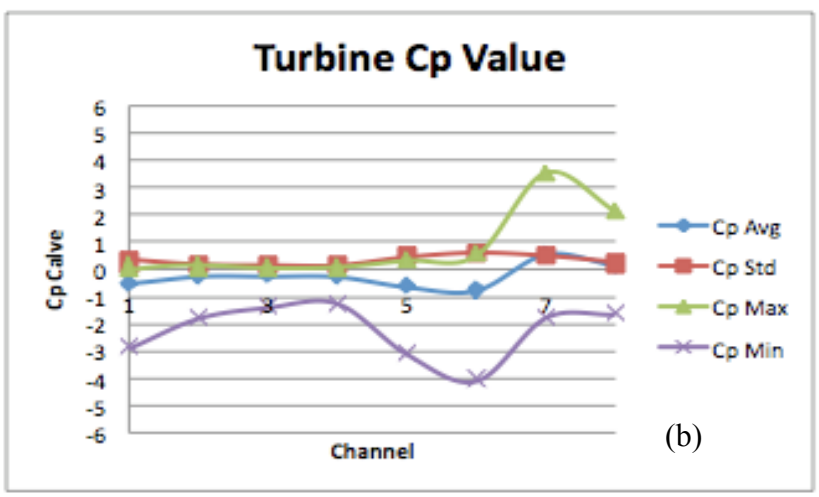

Figure 22. C_p values for "0" degree angle of attack

2) For “15” degree angle of attack:

a) The turbine graph (Figure 23a) shows that the maximum pressure coefficient occurred at tap 7, having a value of approximately 2.8. Taps 5, 6, and 7 measured positive mean Cp values as they were on the windward side of the vent. The remaining taps demonstrate suction pressure coefficients; with tap 8 having the maximum suction coefficient of -3.2.

b) The gooseneck results (Figure 23b) show the maximum pressure coefficient occurred at windward tap 14, with a value of approximately 2.3. This value is the maximum positive pressure coefficient on the gooseneck among all the angles tested. Taps 12, 13 & 14, all on the windward side of the vent at 15 degrees, show positive pressure coefficients. The remaining taps experienced suction as shown in the figure. Tap 10, located on the inclined top face of the vent experienced the peak suction value of -3.2.

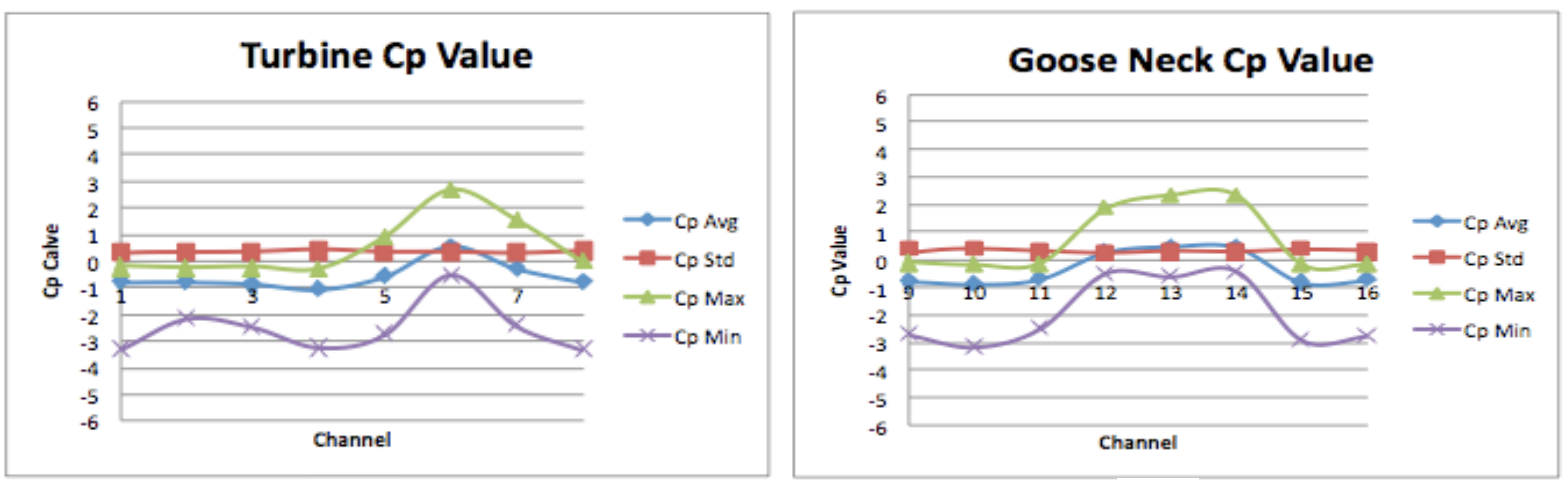

(a) (b)

Figure 23. C_p values for “15” degree angle of attack

3) For “45” degree angle of attack:

a) The turbine graph (Figure 24a) shows that the maximum pressure coefficient occurred at tap 6, having a value of approximately 2.8. Taps5, 6 and 7 measured positive mean Cp values, as they were on the windward side of the vent. The remaining taps demonstrated suction pressure coefficients, with tap 1 having the maximum suction coefficient of -3.2.

b) The gooseneck results (Figure 24b) show the maximum pressure coefficient occurred at windward tap 14, with a value of approximately 2.5. Taps 12, 13 & 14, all on the windward side of the vent at 45 degrees, showed the positive pressure coefficients. The remaining taps experienced suction. Tap 10, located on the inclined top face of the vent experiences the peak suction value of -3.2.

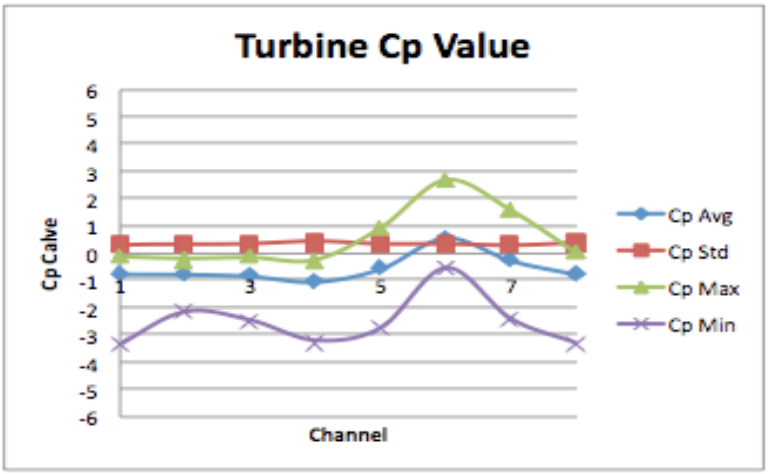

(a)

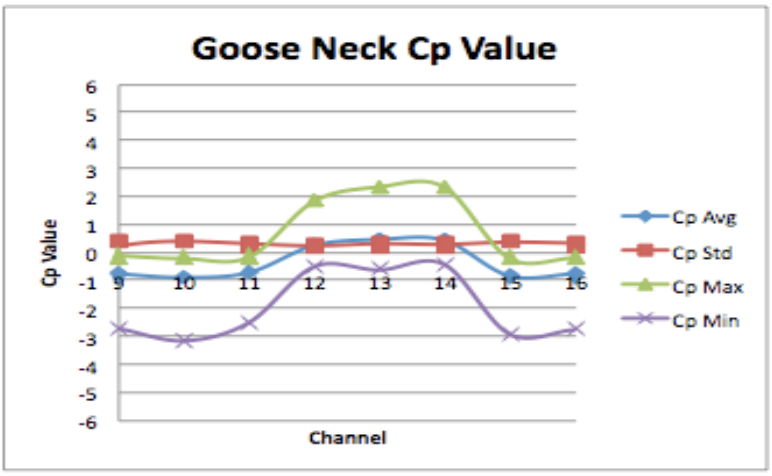

(b)

Figure 24. C_p values for “45” degree angle of attack

4) For “75” degree angle of attack:

a) The turbine graph (Figure 25a) shows that the maximum pressure coefficient occurred at tap 5, having a value of approximately 2.3. Taps 5 & 6 measured positive mean Cp values, as they were on the windward side of the vent. The remaining taps demonstrated suction pressure coefficients; with tap 4 having the maximum suction coefficient of -3.1.

b) The gooseneck results (Figure 25b) show the maximum pressure coefficient occurred at windward tap 12, with a value of approximately 2.9. Taps 12, 13 & 14, all on the windward side of the vent at 75 degrees, showed positive pressure coefficients. The remaining taps experienced suction. Tap 10, located on the inclined top face of the vent experienced the peak suction value of -3.1.

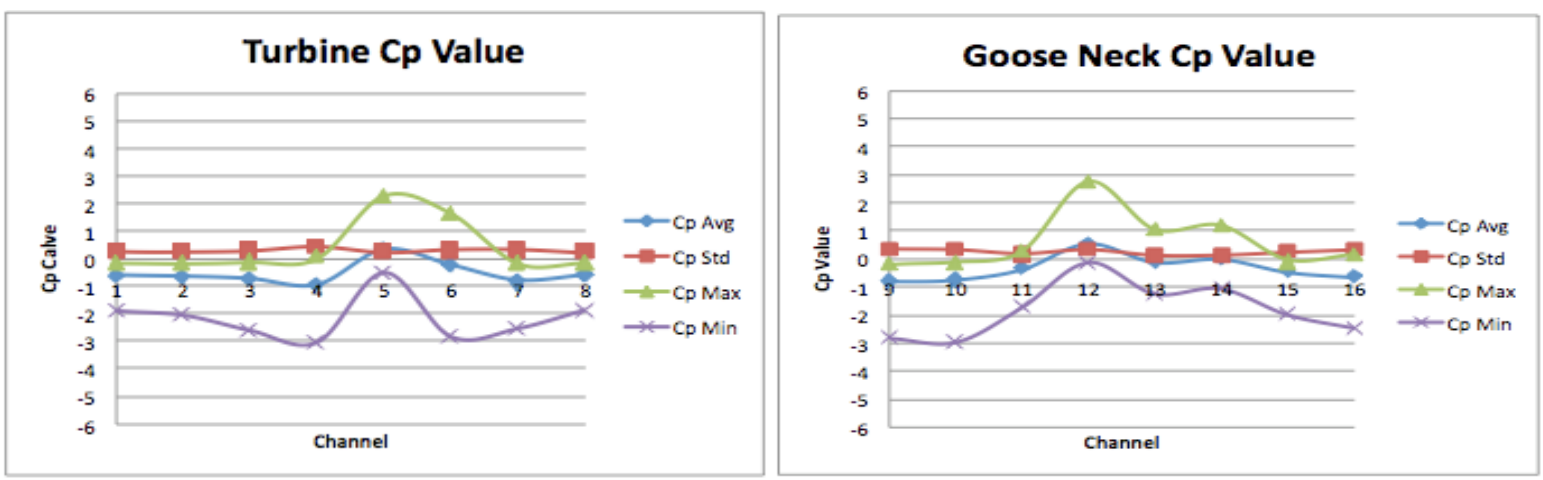

(a) (b)

Figure 25. C_p values for “75” degree angle of attack

5) For “90” degree angle of attack:

a) The turbine graph (Figure 26a) shows that the maximum pressure coefficient occurred at tap 5, having a value of approximately 2.2. Taps 5 & 6 measured positive mean Cp values, as they were on the windward side of the vent. The remaining taps demonstrated suction pressure coefficients; with tap 4 having the maximum suction coefficient of -2.9.

b) The gooseneck results (Figure 26b) show the maximum pressure coefficient occurred at windward tap 12, with a value of approximately 2.5. Taps 12, 13, 14, 15 & 16, all on the windward side of the vent at 90 degrees, show positive pressure coefficients. The remaining taps experienced suction. Tap 9, located on the top face of the vent experienced the peak suction value of -3.1.

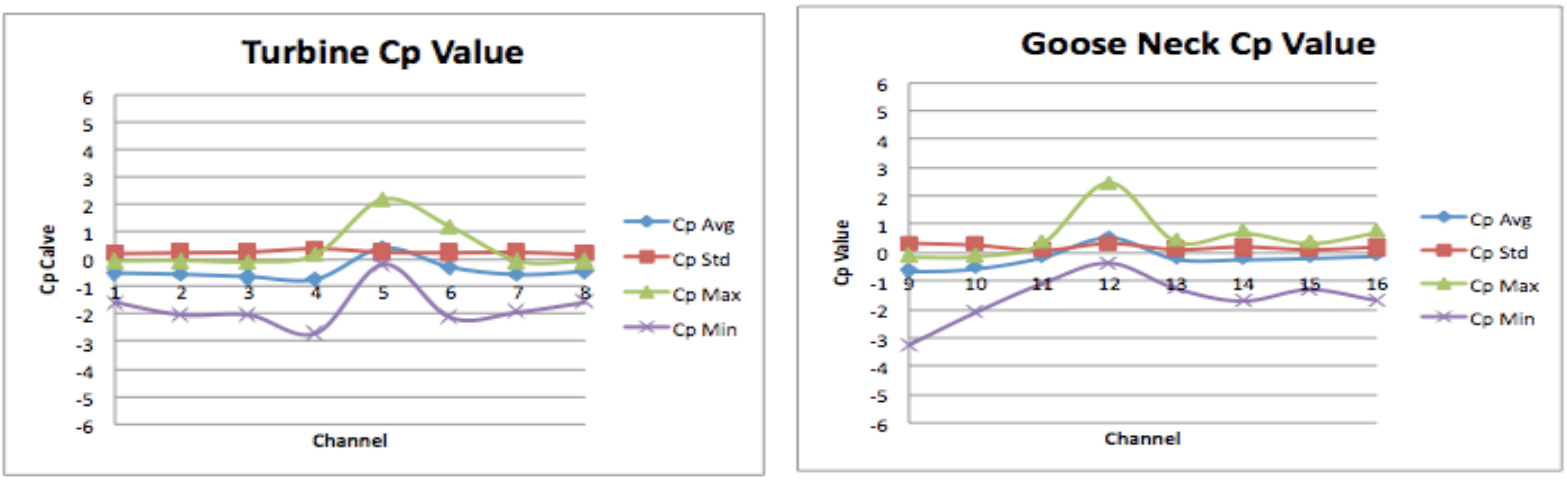

(a) (b)

Figure 26. C_p values for “90” degree angle of attack

5.1.2 Visualization of Turbine Pressure Coefficients for Gable Roof:

a) For "0" degree angle of attack:

It appears from the graph that the gable roof does not allow a symmetric pressure distribution around the vent. Figure 27 shows for 0 degree angle of attack negative and positive pressure coefficients on the turbine vent. The leeward sides of the turbine show a good symmetry where as the windward side does not.

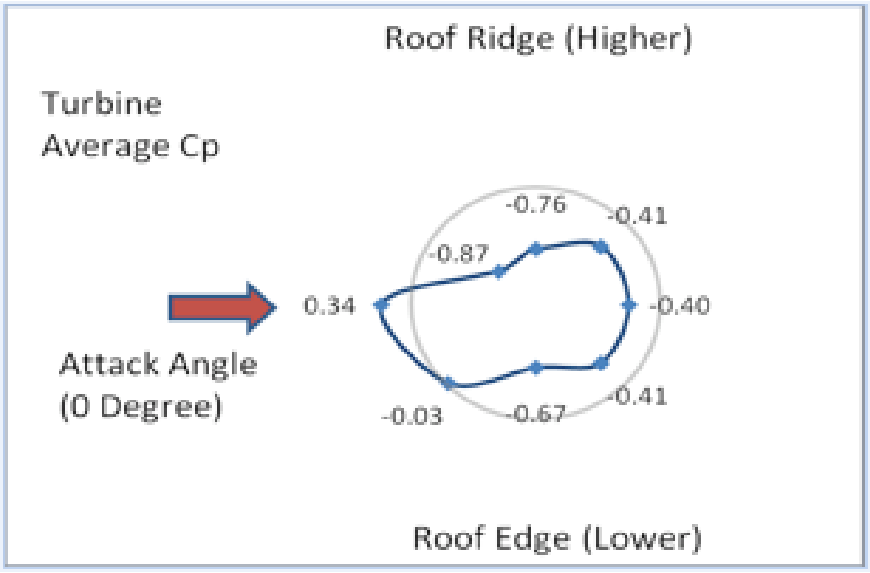

Figure 27. Average C_p values for angle of attack at 0 degree

b) For "15" degree angle of attack:

Figure 28 shows for 15 degree angle of attack negative and positive pressure coefficients on the turbine vent. It appears from the graph that the gable roof specimen does not allow a symmetric pressure distribution around the vent. The leeward sides of the turbine show some symmetry where as the windward side does not.

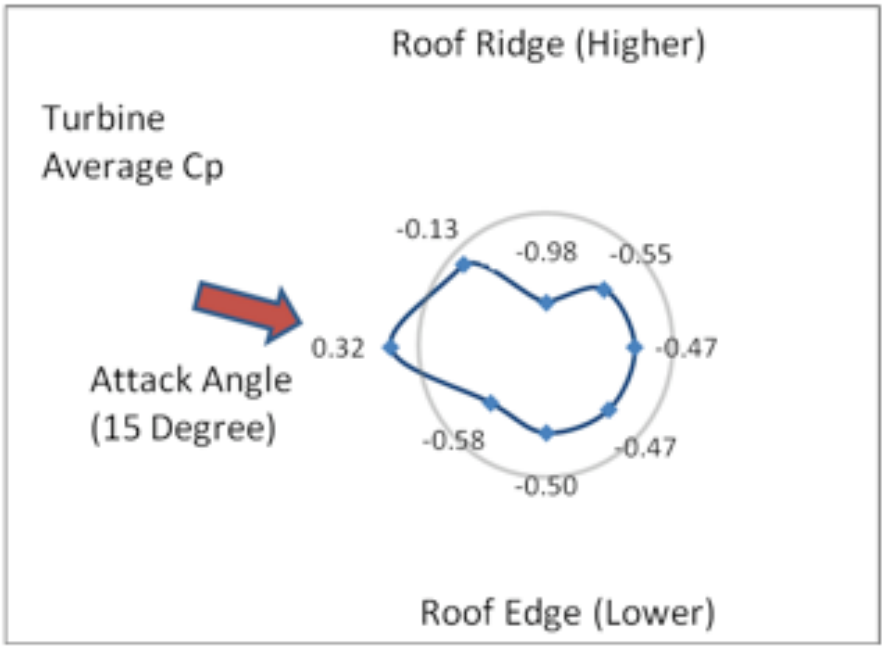

Figure 28. Average C_p values for angle of attack at 15 degree

c) For "45" degree angle of attack:

Figure 29 shows for 45 degree angle of attack negative and positive pressure coefficients on the turbine vent. Similar to the earlier cases the leeward sides of the turbine show somewhat good symmetry as compared to the windward side.

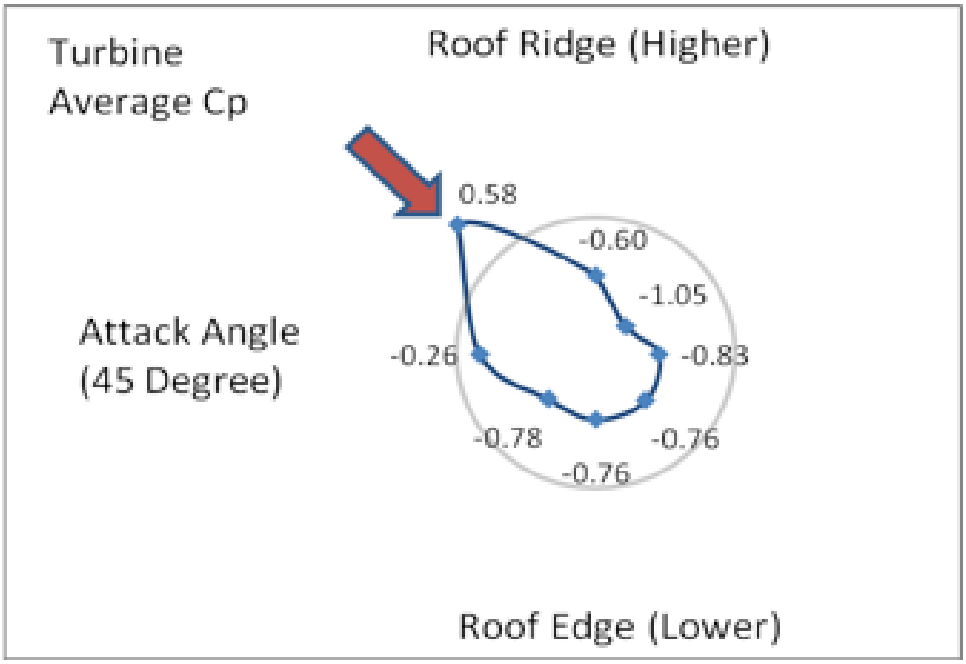

Figure 29. Average C_p values for angle of attack at 45 degree

d) For "75" degree angle of attack:

Figure 30 shows for 75 degree angle of attack negative and positive pressure coefficients on the turbine vent.

Figure 30. Average C_p values for angle of attack at 75 degree

e) For "90" degree angle of attack:

Figure 31 shows for 90 degree angle of attack negative and positive pressure coefficients on the turbine vent.

Figure 31. Average C_p values for angle of attack at 90 degree

5.1.3 Hip Roof Results:

Figure 32 to 36 shows the mean, standard deviation, maximum and minimum pressure coefficients. The pressure coefficient toward the wind direction is the greatest. The maximum pressure coefficient value is found to be +4.0 at an angle 0 degree and the minimum pressure coefficient occurring at an angle 0 degree is -3.9.

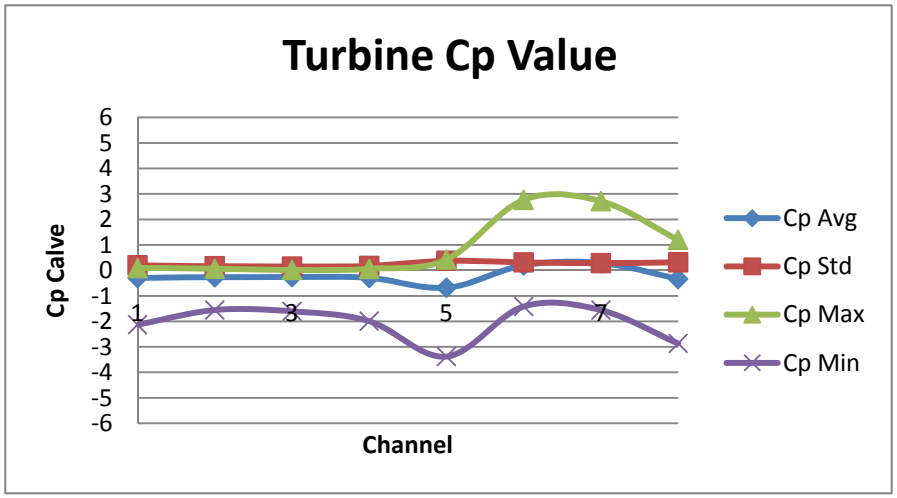

(a)

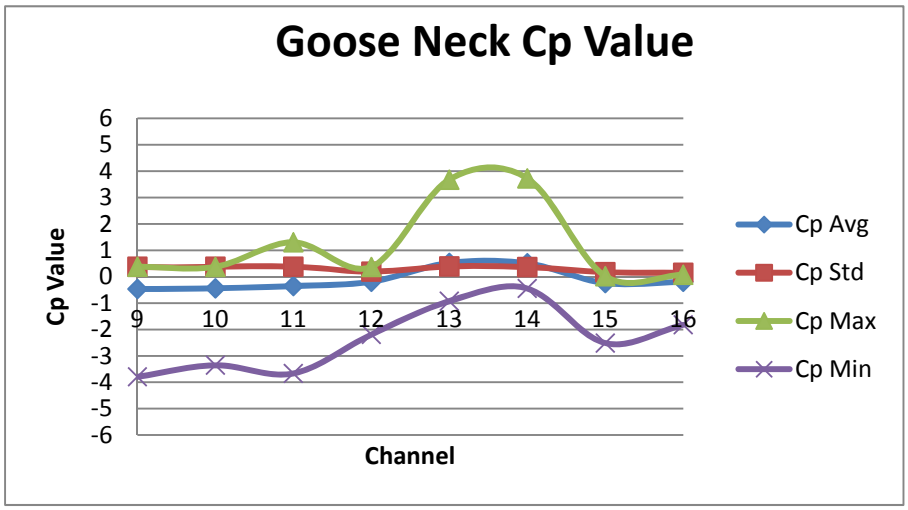

(b)

Figure 32. C_p values for "0" degree angle: (a) turbine vent, (b) gooseneck vent

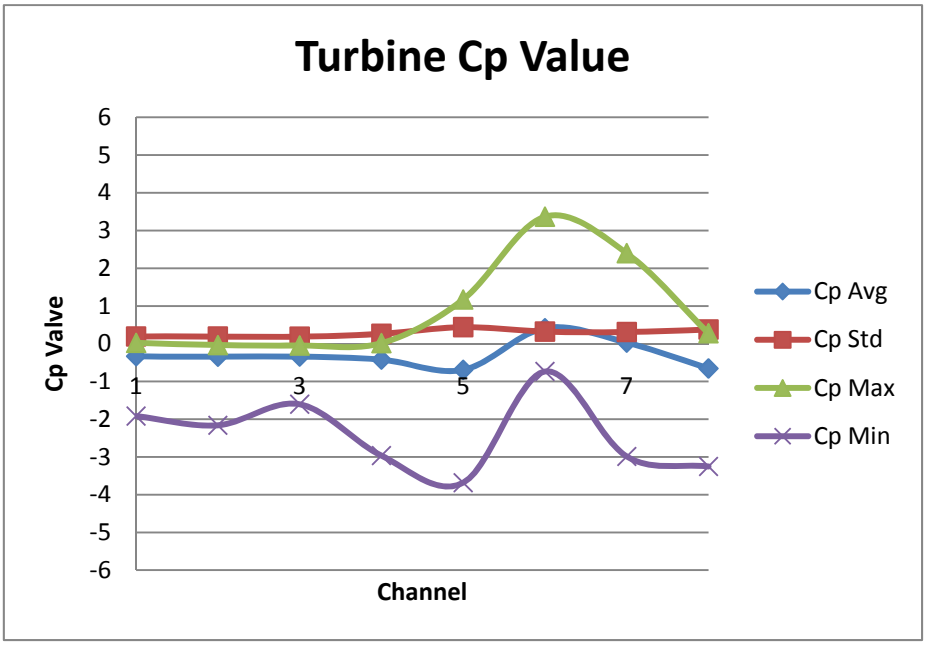

(a)

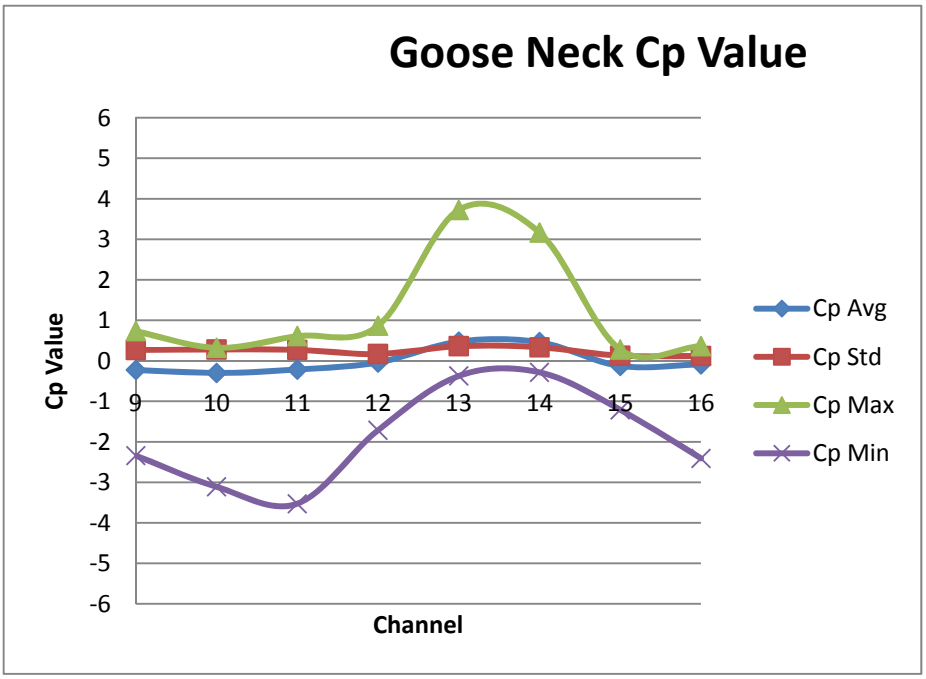

(b)

Figure 33. C_p values for "15" degree angle: (a) turbine vent, (b) gooseneck vent

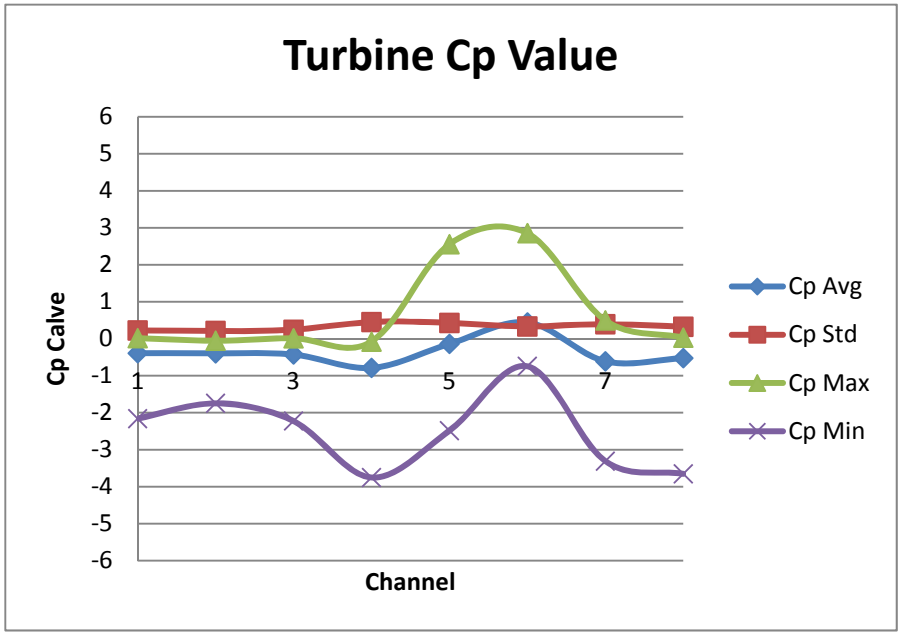

(a)

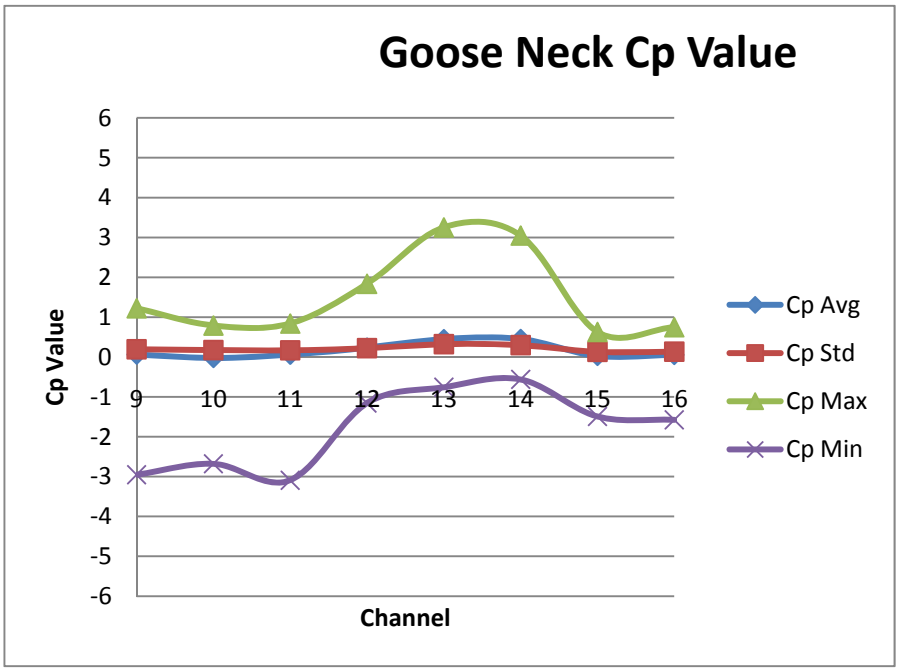

(b)

Figure 34. C_p values for "45" degree angle: (a) turbine vent, (b) gooseneck vent

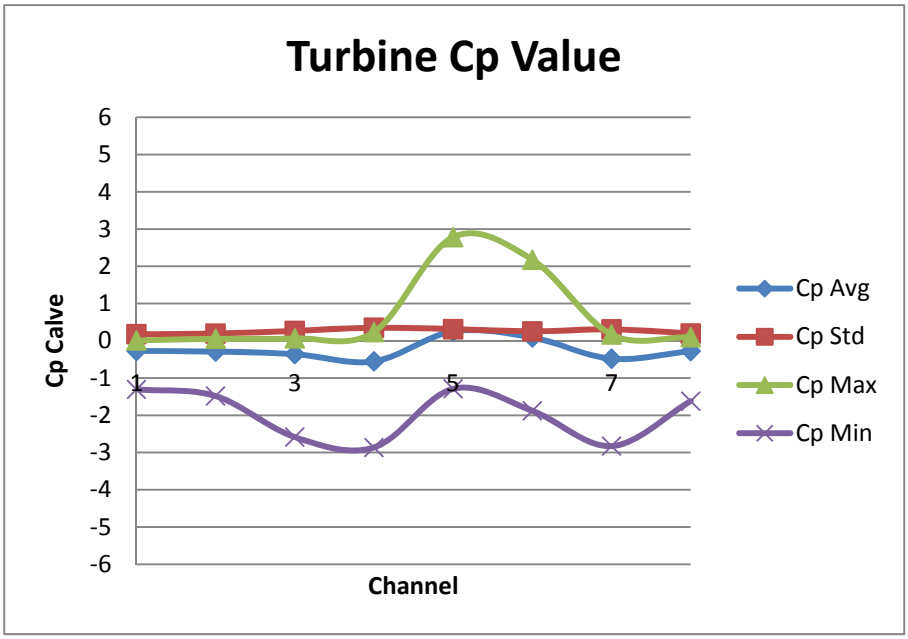

(a)

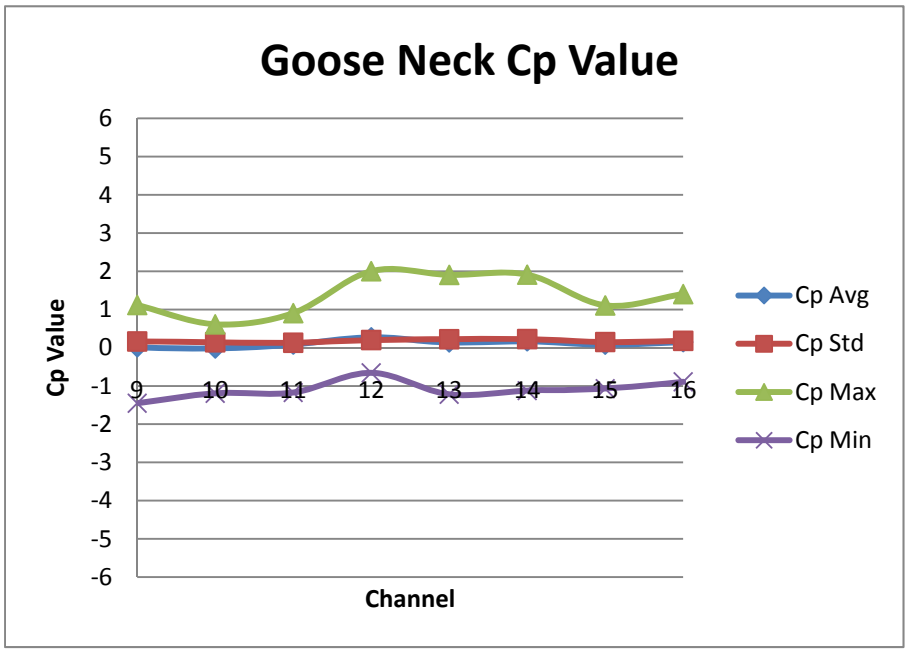

(b)

Figure 35. C_p values for "75" degree angle: (a) turbine vent, (b) gooseneck vent

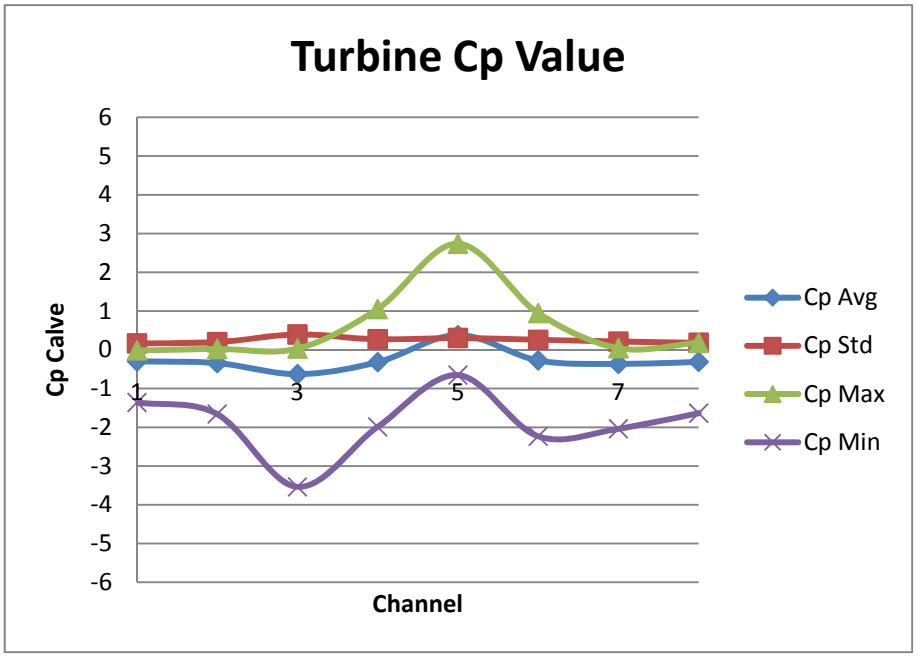

(a)

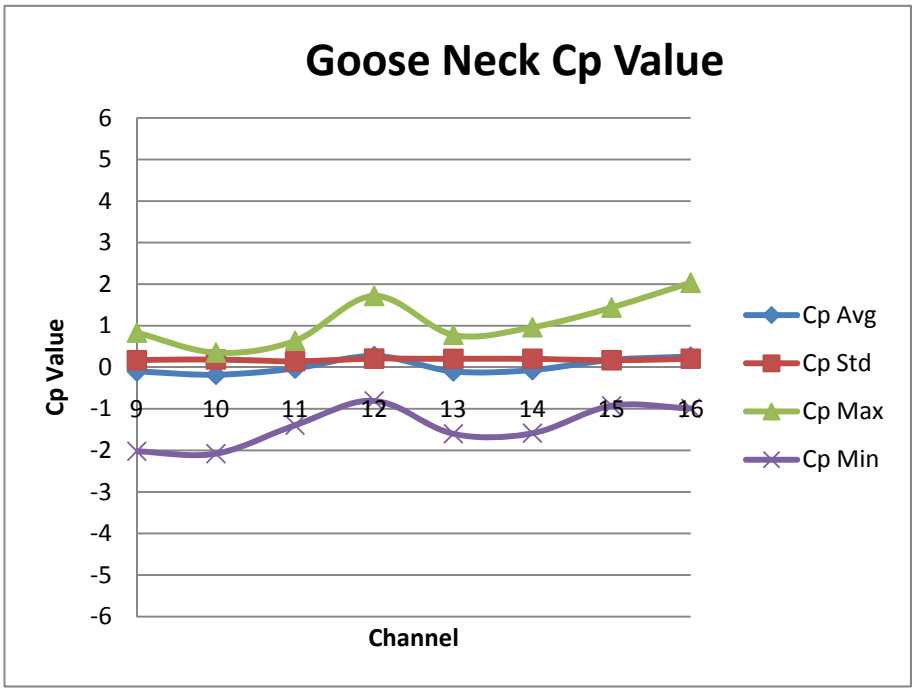

(b)

Figure 36. C_p values for "90" degree angle: (a) turbine vent, (b) gooseneck vent

5.2 Water Intrusion Test Results:

Water intrusion tests were also conducted to evaluate the performance of different ventilation systems regarding rain water infiltration. Two water rates were used in the gable roof water tests, one is 9 inch/hr and another one is 19 inch/hr. Only 19 inch/hr was used for the hip roof water intrusion test. The amount of water intrusion and the differential pressure coefficients ΔCp (difference of external and internal pressure coefficients) are compared in this section. Figures 37 and 39 show the water intrusion tests results. Figures 38 and 40 show the differential pressure coefficients. There was no water infiltration through the ridge and soffit vents for gable roof. However, there was small amount of water infiltration through the ridge vent on hip roof at 90 degree wind attack angle. In addition, there are no significant changes in water infiltration through the turbine vent for different wind angles.

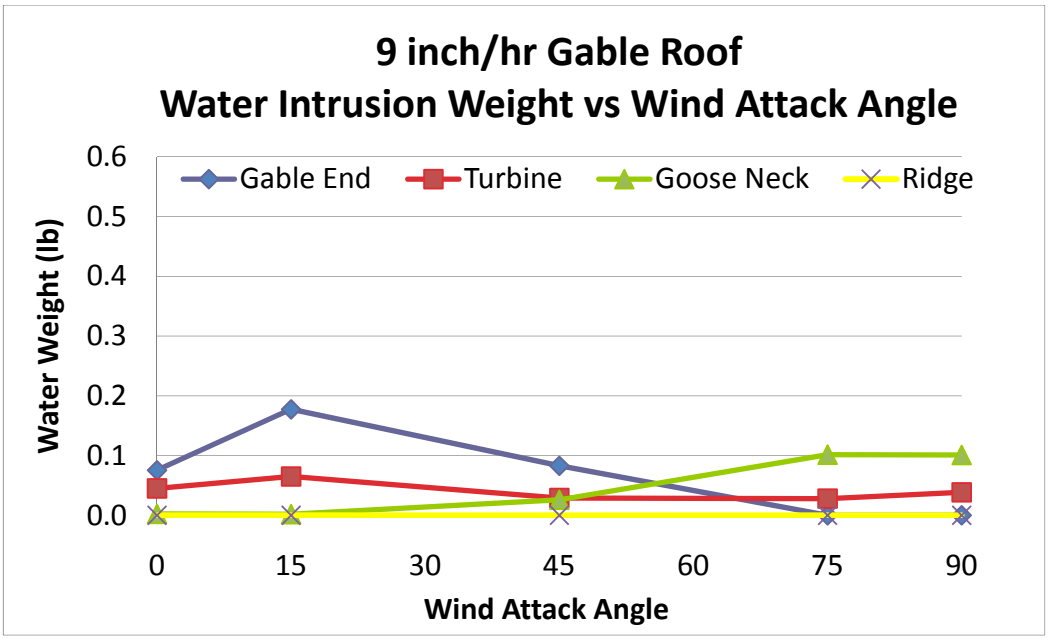

(a)

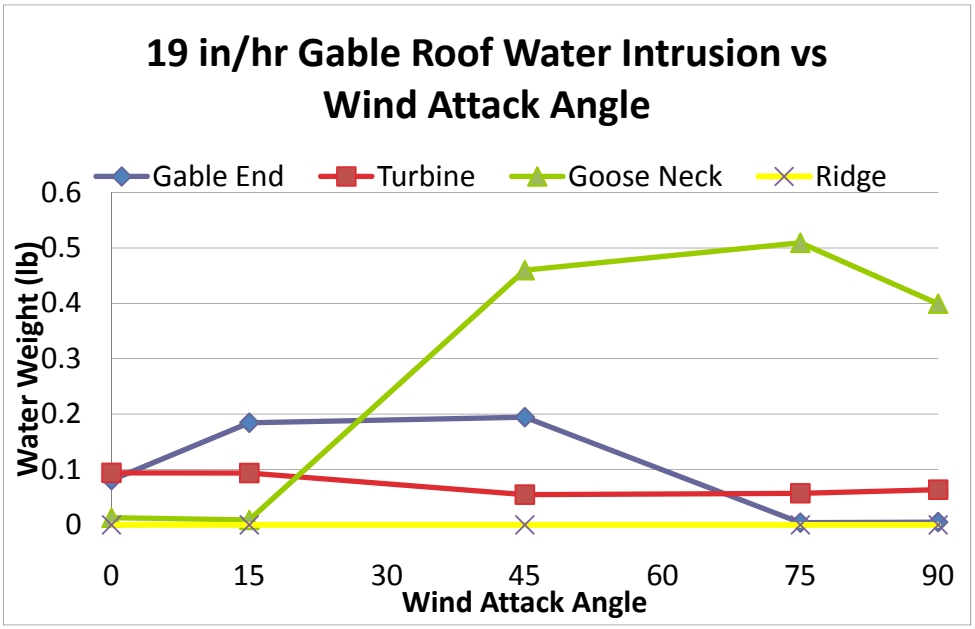

(b)

Figure 37. Water intrusion test results for gable roof: (a) 9 in/hr, (b) 19 in/hr

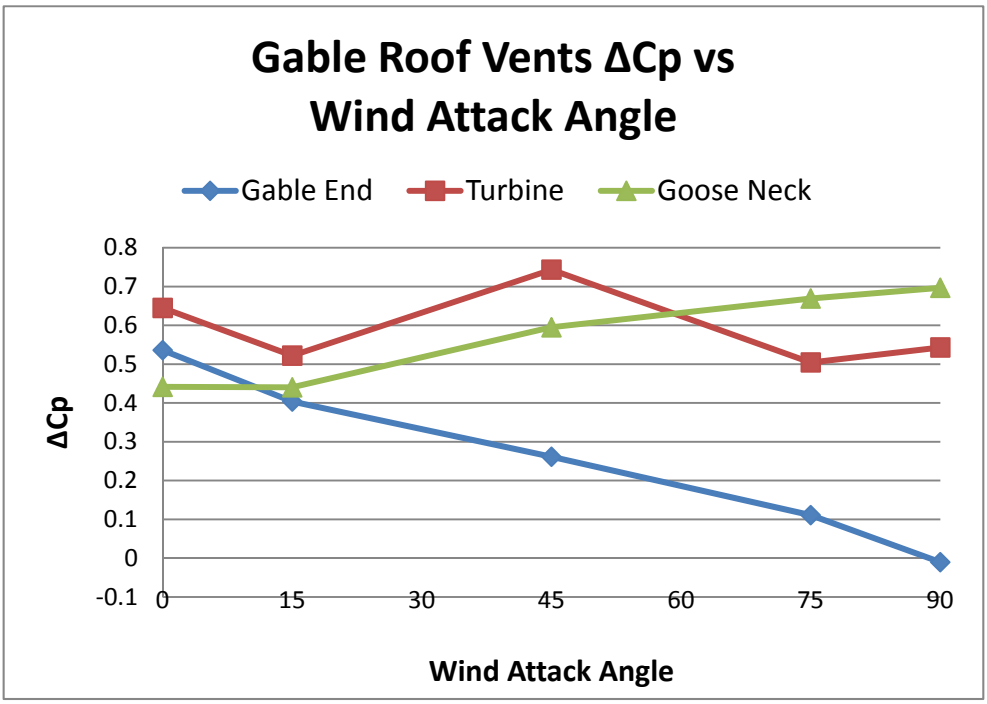

Figure 38. ΔCp values for gable roof specimen vents

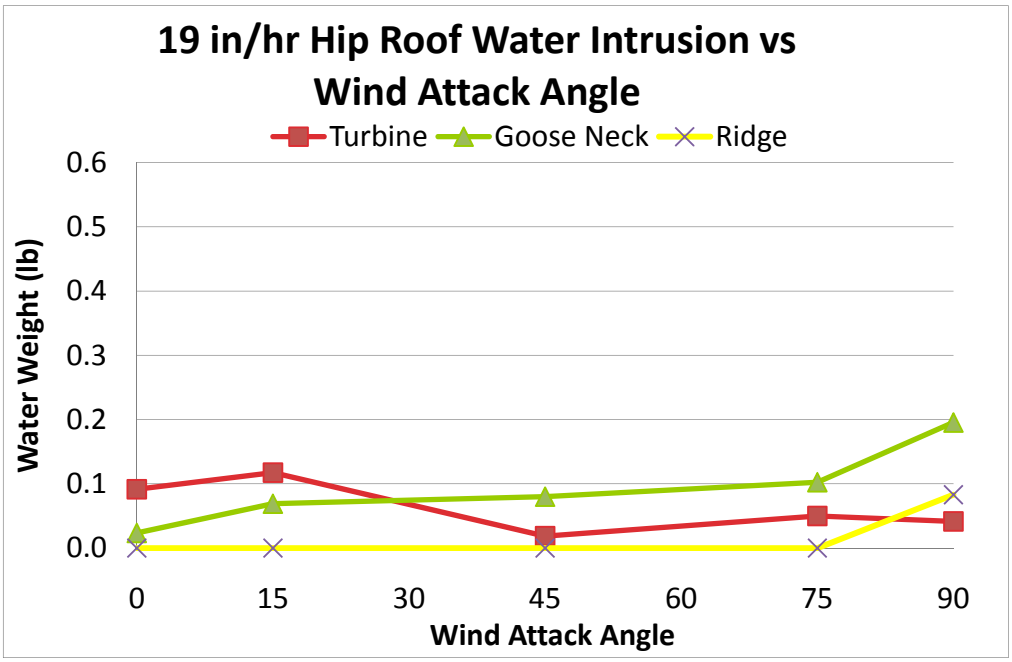

Figure 39. Water intrusion test results for hip roof for 19 inch/hr

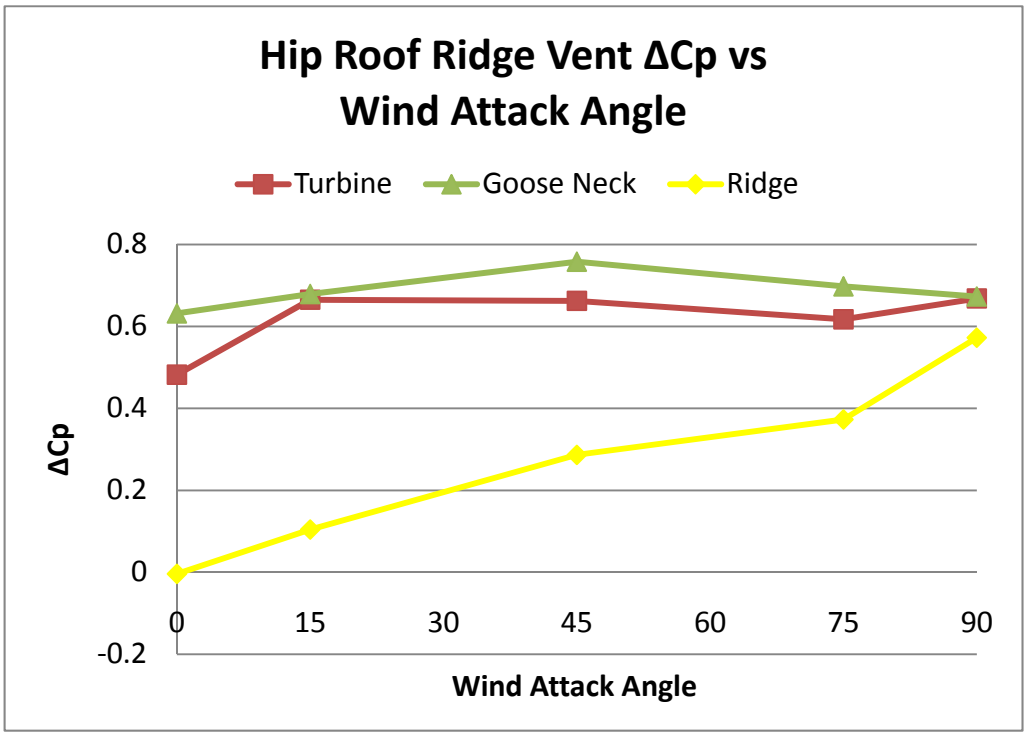

Figure 40. ΔCp values for hip roof specimen vents

Figures 37 to 40 show somewhat similar trends between the water infiltration amount and the ΔCp values for each type of vent. This means that water intrusion amount can be correlated to the ΔCp values. As the value of certain ΔCp increases, there will be more water infiltration through a vent. The water amount collected by gable end and goose neck vents varied with the wind attack angle as shown in Figures 37 to 40. This is because both types of the vents have frontal openings. The water amount will increase if the wind attack angle is aimed to the vent frontal openings. However, it was observed that at "0" degree angle of attack the amount of water infiltration through the gable end vent was not the maximum. This may be due to the mechanism of the gable end vent. Figure 41 shows the gable end vent with the blinds. When the water came from perpendicular direction of the vent surface, the blinds could block some amount of the water from getting into the vent.

Figure 41. Gable end vent

Figures 42 and 43 show the ΔCp values of soffit and rigde vents on gable roof specimen. Most of the ΔCp values are less than 0.1 and all of the ΔCp values are less than 0.15. The low ΔCp values explain why there was no water intrusion for the soffits and ridge vents in the gable roof tests.

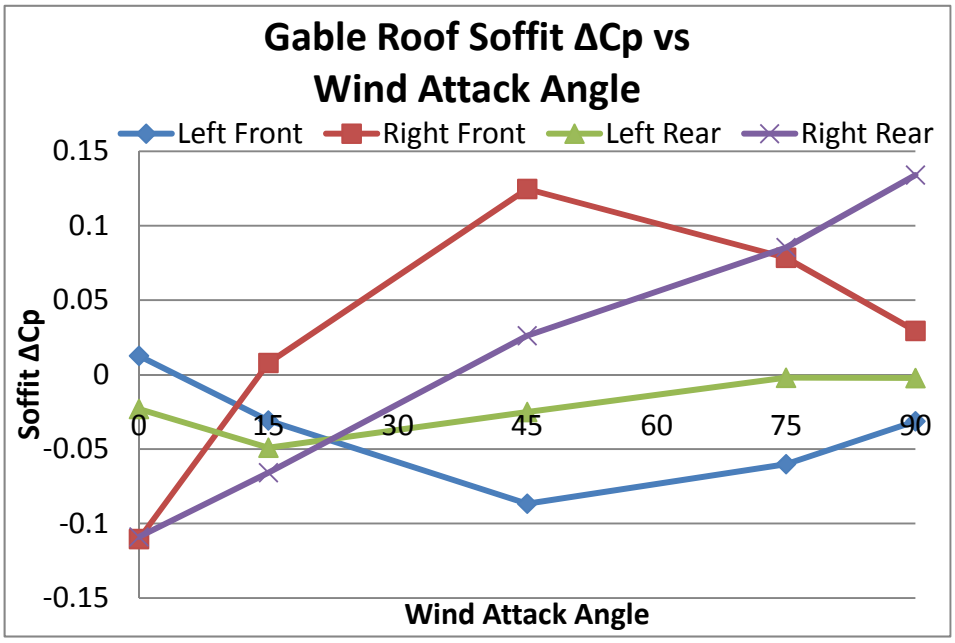

Figure 42. ΔCp values for soffit vents for gable roof specimen

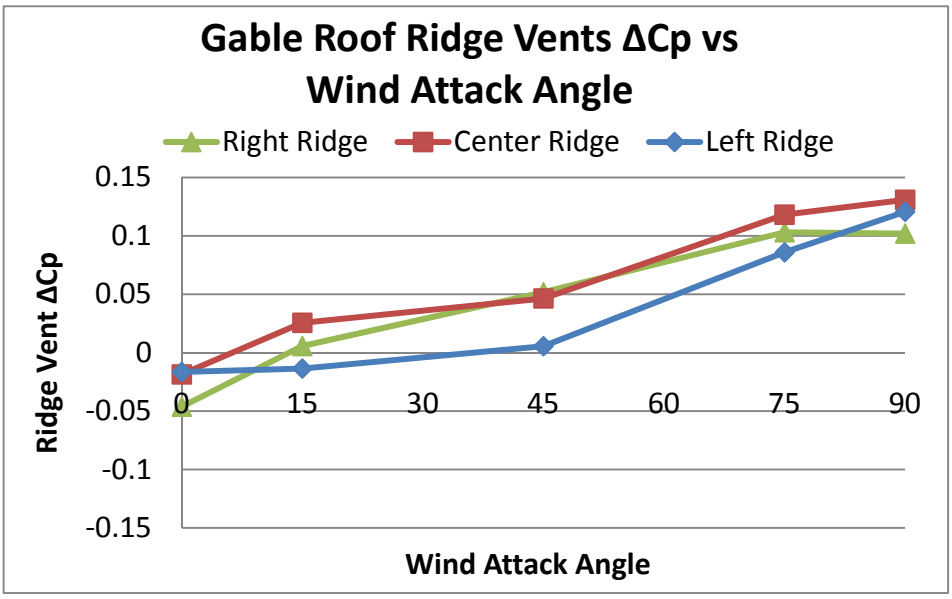

Figure 43. ΔCp values for ridge vents for gable roof specimen

Figure 44 shows the ΔCp values for soffit vents for the hip roof specimen. Since most of the values are negative, there will be no water intrustion for these soffit vents.

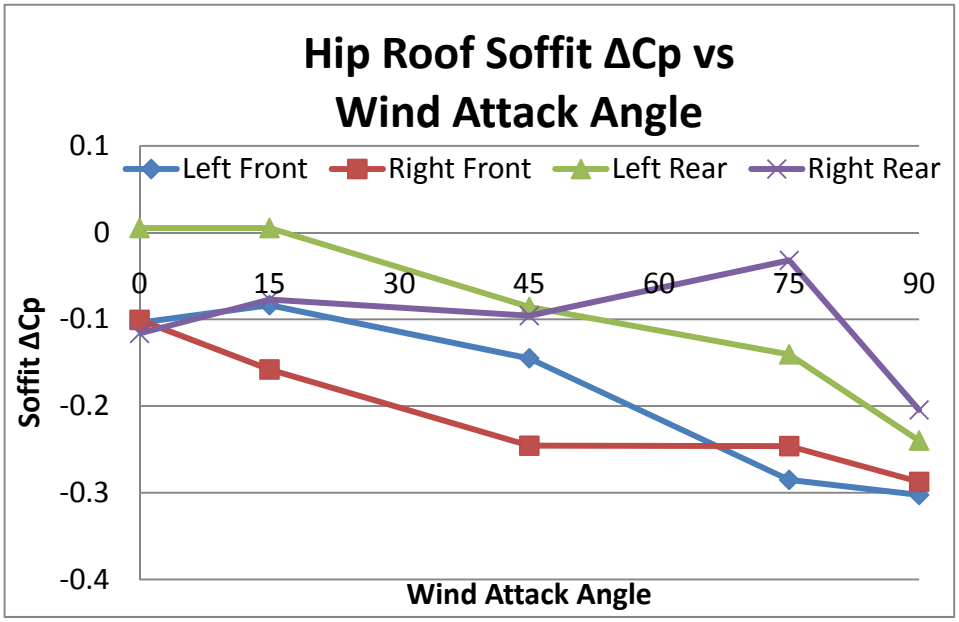

Figure 44. ΔCp values for soffit vents for hip roof specimen

Figure 45 shows the ΔCp values for ridge vents on hip roof specimen. It was noticed that there was some water coming through the ridge vent at 90 degree wind attack angle (Figure 39 the yellow curve). Figure 45 also shows that at 90 degree wind attack angle, the ΔCp increased to 0.6 sharply which increased the chances for water infiltration.

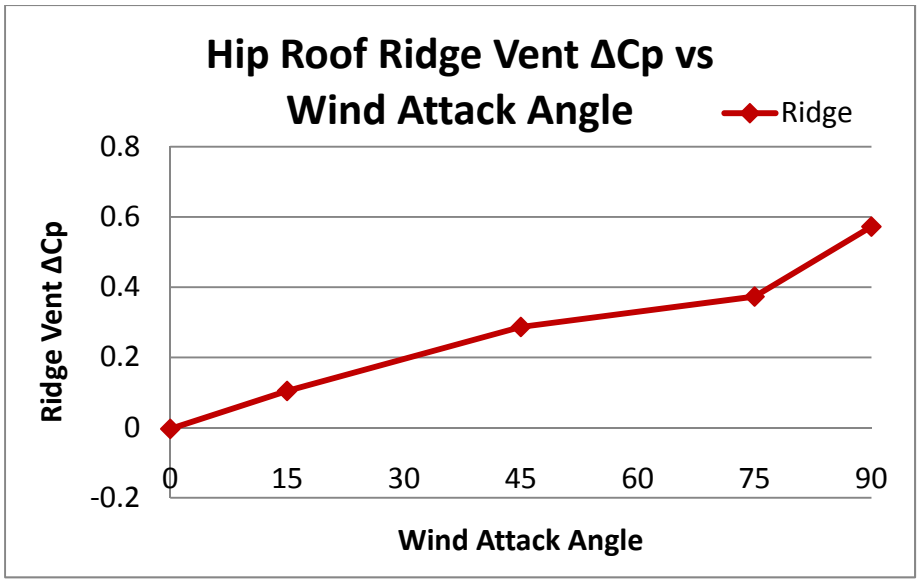

Figure 45. ΔCp values for ridge vent for hip roof specimen

5.3 Influence of Reynolds Number on Pressure Distribution over Cylindrical Vent with Circular Cross Section (Turbine Vent)

Drag coefficient is a function of Reynolds number (Re) (Simiu and Scanlan, 1996). Figure 46 shows typical curve for drag coefficients C_d vs Re. In the current pressure testing, the Re has been calculated as: Re = 67000 x V x L. Where V is the mean wind speed at men roof height and L is the dimension of the object. In our case, L can be considered as the diameter of turbine which is 12 inch (0.305m). Therefore, the Re = 67000 x 20.27 m/s x 0.305m = 4.14 x 10^5 and the corresponding C_d value is 0.32

(Figure 46). However, as the Re decreases below 4 x10^5, the C_d value increases sharply, e.g., C_d = 1.1for Re=2 x 10^5.

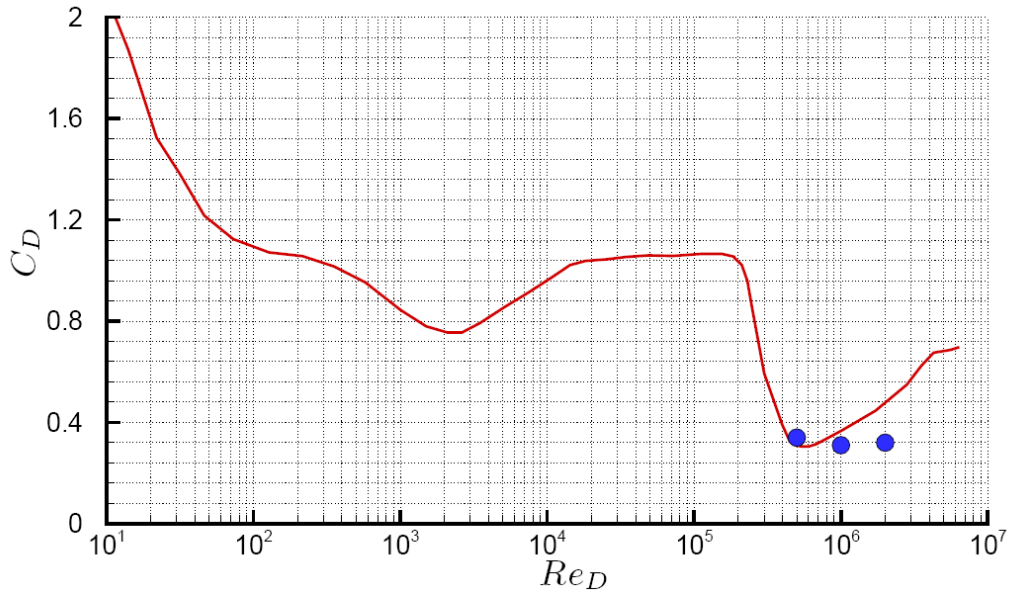

Figure 46. Drag Coefficient as a function of Reynolds number (Wang, 2001)

Figure 47 shows the pressure coefficients over the turbine circumstantial surface. Compared to the results presented by Simiu and Scanlan (1996), the data obtained from Wall-of-Wind is close to that for Re = 1.1 x 10^5. In addition, the C_p values for hip roof test are smaller than the C_p values for gable roof test.

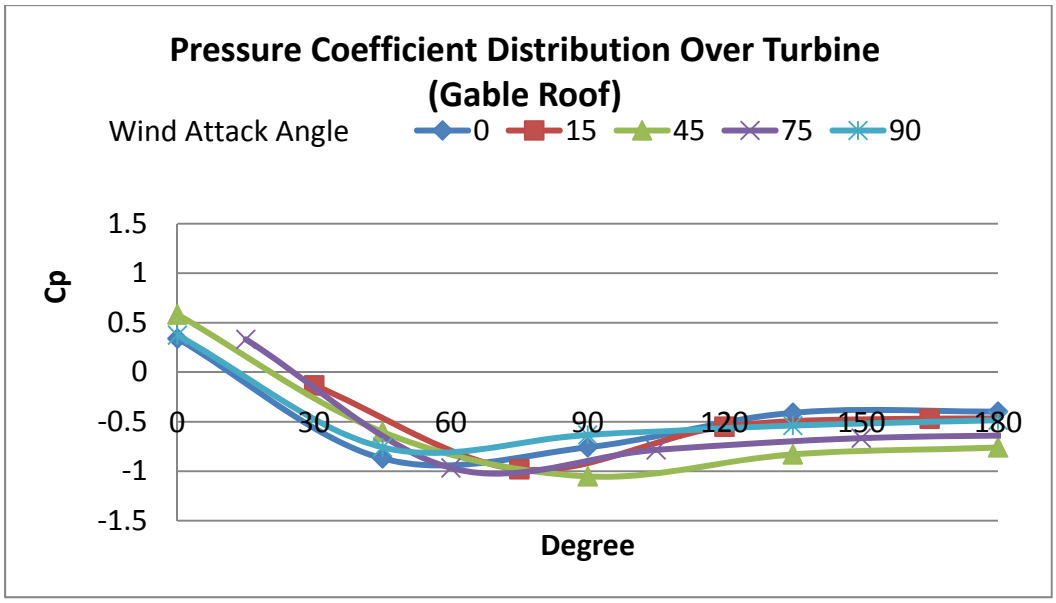

Figure 47. (a) Cp values distribution along turbine vent for gable roof

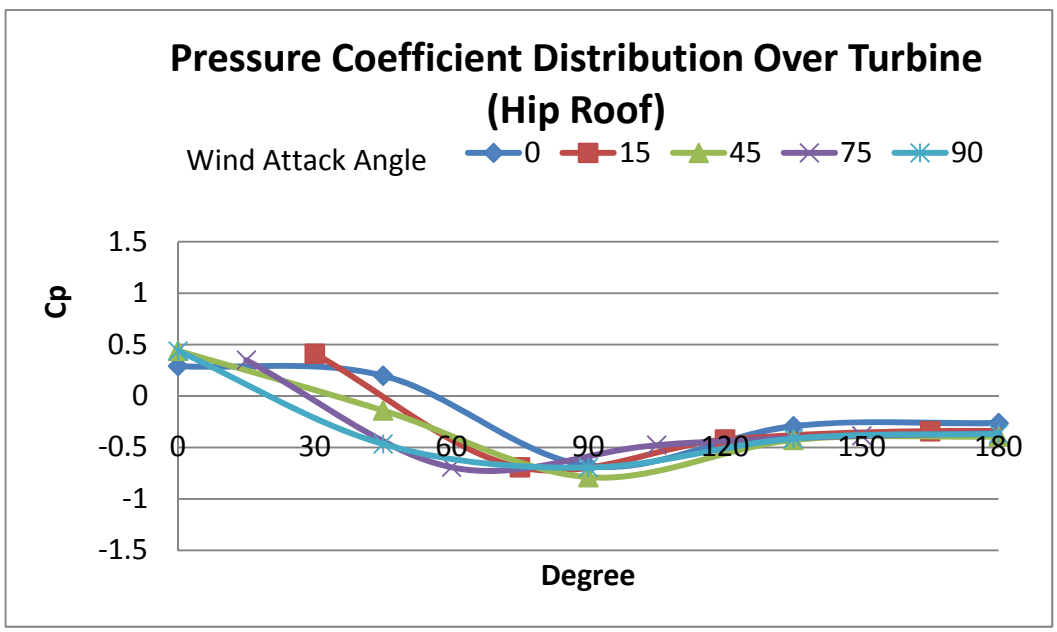

Figure 47. (b) Cp values distribution along turbine vent for hip roof

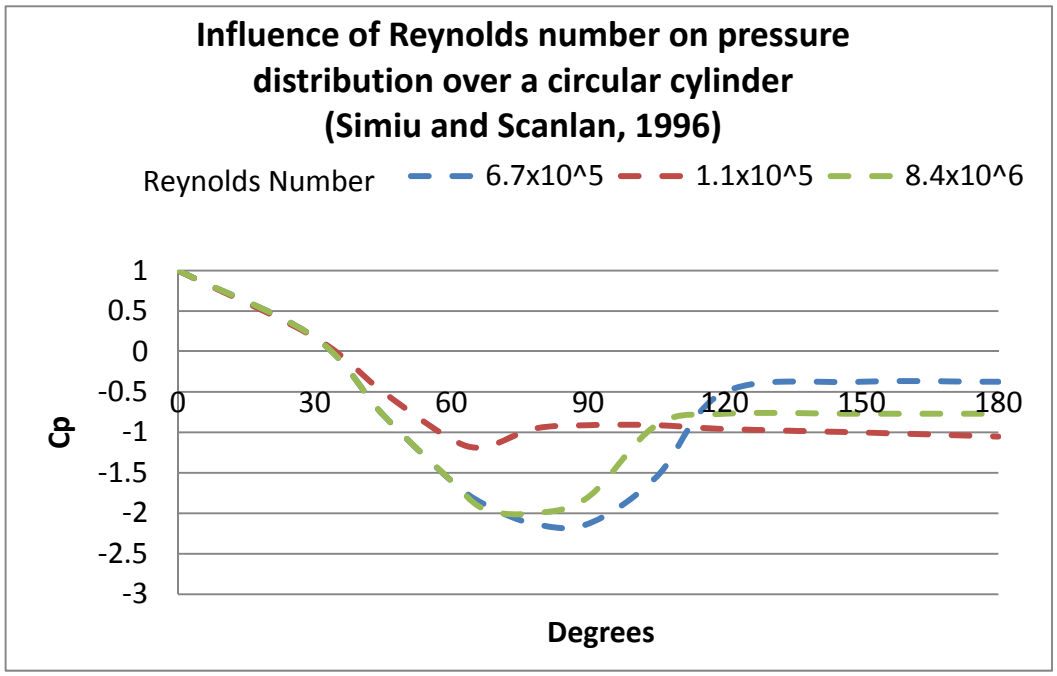

Figure 47. (c) Cp values distribution along Circular cylinder (Simiu and Scanlan, 1996)

5.4 Uplift and Drag Coefficients

5.4.1 Uplift Coefficient

The uplift coefficients C_L are also calculated for goose neck vent and shown in Figure 48. In the figure, the C_L values observed for gable and hip roofs are not only different at the minimum values, but also the trends of the curves are quite dissimilar. For hip roof, goose neck vent is subjected to uplift forces from all wind attack angles. However, for the gable roof, goose neck vent is only subjected to uplift forces at 0 and 15 degree wind attack angles. At 45, 75, and 90 degree wind attack angles, goose neck is subjected to push down forces.

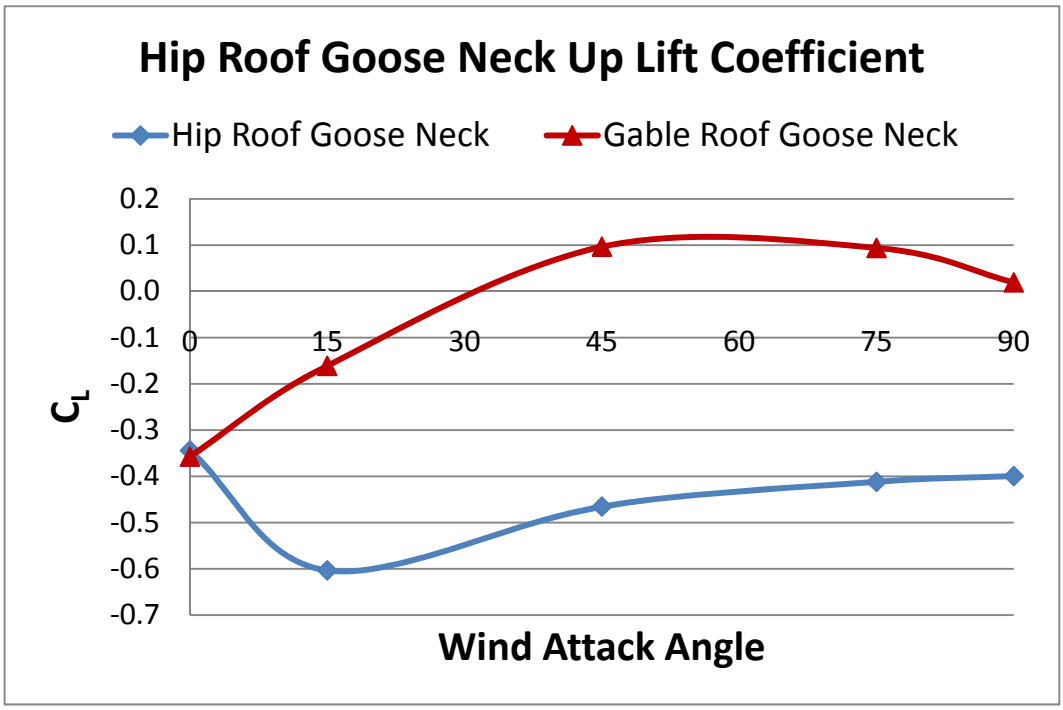

Figure 48. Goose neck vent uplift coefficients for gable roof and hip roof

5.4.2 Drag Coefficient

The turbine vent drag coefficient for different wind attack angles on both gable roof and hip roof are shown in Figure 49. For gable roof, C_d coefficient is between 0.3 and 0.75. For hip roof, the C_d value for turbine vent is about 0.3. The maximum goose neck vent C_d value is 1.25 on gable roof and 0.75 on hip roof. It is noticed that both turbine and goose neck vents are subjected to higher C_d values on the gable roof. For the hip roof, the maximum C_d values of turbine and goose neck vents are about half of the C_d values for the gable roof. By comparing the C_d values for turbine which are between 0.3 and 0.7 with the C_d values in Figure 46, the Re obtained from Figure 46 is between 3 x 10^5 and 5 x 10^5. This range includes the Re value calculated previously as 4.14 x 10^5 for current testing.

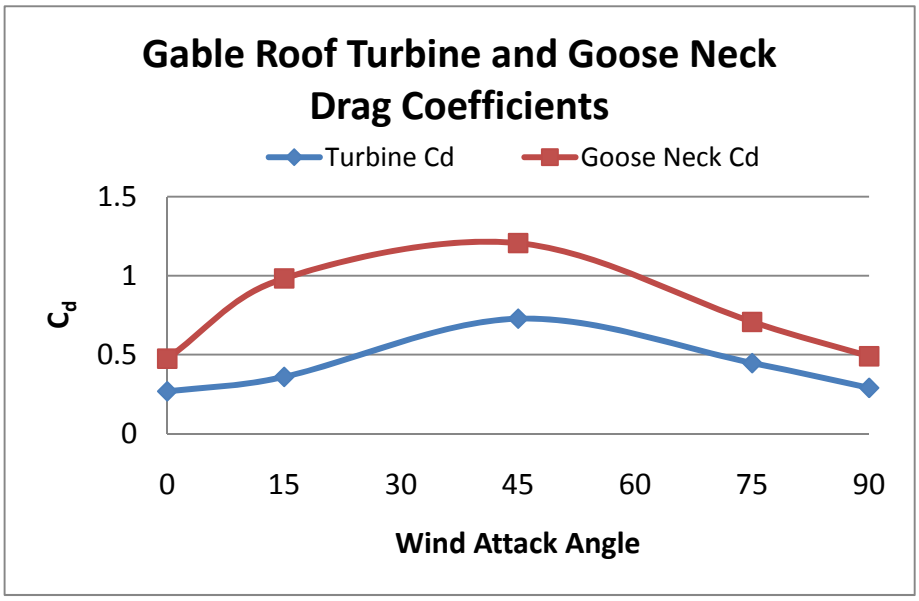

(a)

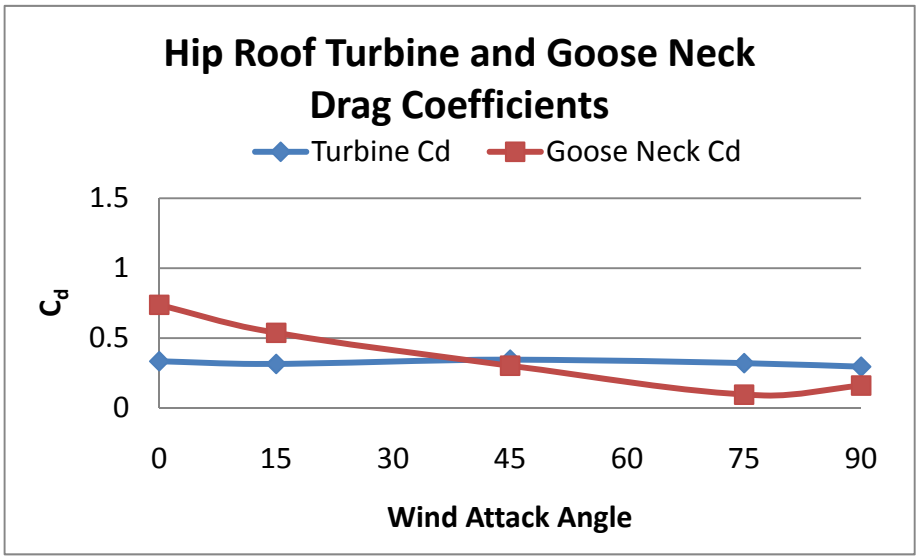

(b)

Figure 49. Vent drag coefficients for gable roof and hip roof

6. CONCLUSIONS:

The tests indicate that water infiltration through a vent system is dependent upon the differential pressure as well as the vent mechanism. For vents experiencing higher differential pressures, cost effective vent covers can be used during storms to reduce water infiltration. Active controls can also be designed to close the vents automatically as differential pressure increases based on the wind speed and wind angle of attack. The later strategy is a topic of future research.

Based on the results the current full-scale test protocol developed for testing vents seems to be an effective method to relate the water intrusion through vents to the differential pressure across the vents. The tests generate realistic aerodynamic loads on the holistic building models incorporated with various vents. Such aerodynamic loads dictate the differential pressures which are the driving factors for water intrusion through the vents. Future study should include comparison of current test protocol with that indicated in the Florida Building Code. This will help in determining the adequacy of test protocols given in the code and suggest necessary modifications.

Based on the test results, in general, the overall volume of water intrusion between 0 and 30 degrees angles of attack was significantly smaller than that for angles of attack between 45 through 90 degrees. This can be attributed to the gooseneck vent, which allowed the most water to enter between 45 and 90 degrees. This is because the opening on the gooseneck was facing the wind for angles of attack between 45 through 90 degrees.

The volume of water intrusion through the gable end vent for perpendicular winds (0 degree) is less than that for slightly oblique winds (say, 15 degree) though the different

pressure is higher for the former case. The reason behind this can be the louver mechanism which doesn't allow perpendicular wind or water to get into it that easily. However at slight inclination the wind-driven rain can get through the opening under the louver. For the gable end vent no water intrusion was seen at 75 degree and 90 degree angles of attack and a linear trend is visible for 15 degree to 75 degree.

Water infiltration through the turbine vent is pretty much consistent and is somewhat independent of the wind angles of attack (angles from 0 degree to 90 degree). As the top of the turbine vent is always spinning at the time of wind attack it lessens water intrusion through it.

For the goose neck vent a consistent trend of increasing water infiltration is observed with the increase in the differential pressure based on the angle of attack. The goose neck vent has maximum water infiltration when the opening on the gooseneck vent faces the wind which allows maximum pressure differentials for angles of attack between 45 through 90 degrees. It is recommended that the goose neck vent should be covered during storms to reduce water infiltration.

For the ridge vent differential pressure coefficient is minimal and no water intrusion is seen for most of the angles of attack (except 90 degree for hip roof for which differential pressure increases abruptly). Similarly, for the soffit vent no water intrusion was seen for any of the angles of attack. This is unusual as soffit vent water intrusion had been observed during many past hurricanes. For the current tests the roof eave inclination might have prevented the water infiltration through the soffit vents (see Fig. 19). Further research is needed in this area to develop methods for reducing water infiltration through soffit vents.

The relationships obtained between Reynolds number and the drag coefficients or pressure coefficients were comparable with previous studies.

7. REFERENCES AND RELATED LINKS:

AIR VENT INC.
[http://www.airvent.com/homeowner/whyVent/whyVent.shtml]

Baffled attic Vent, Richard S. Duncan et al
[http://www.google.com/patents?id=Rt6fAAAAEBAJ]

Blessing, C.M. (2007), "Mitigation of Roof Uplift Through Vortex Sup pressure Techniques" MSc Thesis, Florida International University, Miami, Florida.

Bitsuamlak, G.T., Gan Chowdhury, A., Sambare, D. (2009), "Application of a Full-Scale Testing Facility for Assessing Wind-Driven-Rain Intrusion," Building and Environment, 44 (12), pp. 2430-2441.

Bitsuamlak, G. T., Tecle A. (2009), "Full-Scale External and Internal Pressure Measurements on Low-Rise Building Roofs," Report submitted to IHRC, Research Project funded by The State of Florida Department of Community Affairs.

Florida Building Code 2007.

Huang, P., Gan Chowdhury, A., Bitsuamlak, G. T., Liu, R., (2009), "Development of Devices and Methods for Hurricane Wind Flow Simulation in a Full-Scale Testing Facility," Wind and Structures, 12 (2), pp. 151-177.

Lott, N., and Ross, T., (2006), "Tracking and Evaluating U.S. Billion Dollar Weather Disasters, 1980-2005," Forum on Environmental Risk and Impacts on Society: Successes and Challenges American Meteorological Society.

Liu, R. (2008) "Flow Characterization and Active Control of Turbulence," MSc Thesis, Florida International University, Miami, Florida.

National Academy of Sciences. Meeting research and education needs in coastal engineering. National Academy Press; 1999. pp. 11.

National Science Board (2007), "Hurricane Warning: The Critical Need for a National Hurricane Research Initiative," NSB-06-115.

Owens Corning Roofing. THE PINK PANTHER™ & © 1964-2009 Metro-Goldwyn-Mayer Studios Inc
[http://roofing.owenscorning.com/homeowner/accessories/ventilation/?s_kwcid=roof%20vents%7C2522511830]

Roof and Wall Venting System. Kind Code: A1. Document Number: 20080028704.
[http://www.freepatentsonline.com/y2008/0028704.html?query=Wall+vents&stemming= on]

Roof and Wall Venting System. Kind Code: A1. Document Number: 2007001195. Document type: United States Patent Application.
[http://www.freepatentsonline.com/y2007/0011957.html?query=Wall+vents&stemming= on]

Risk Management Solutions.
[www.rms.com]

Science Directory
[http://www.sciencedirect.com/science?_ob=PublicationURL&_cdi=5715&_auth=y&cct=C000054271&_version=1&_urlVersion=0&_userid=2139759&_pubType=J&md5=628077b0eac596abb0913ff26b275c7f]

Simiu E., Scanlan R. (1996), "Wind Effects on Structures", 3rd edition, New York: Wiley.